AD-A033 506 ILLINOIS UNIV AT URBANA-CHAMPAIGN SAVOY AVIATION DEC ETC MD F/G 9/2 F/G 6/6
DESIGN OF A DIGITAL AIRCRAFT SIMULATOR FOR ARMY AVIATION RESEARCH ... ET
1976 P D BIOLCHINI NCH, J F ROBERTS F33615-73-C-1238
UNCLASSIFIED ARL-76-19/AFAL-76-31 NL NL

1 OF 1
AD A033506

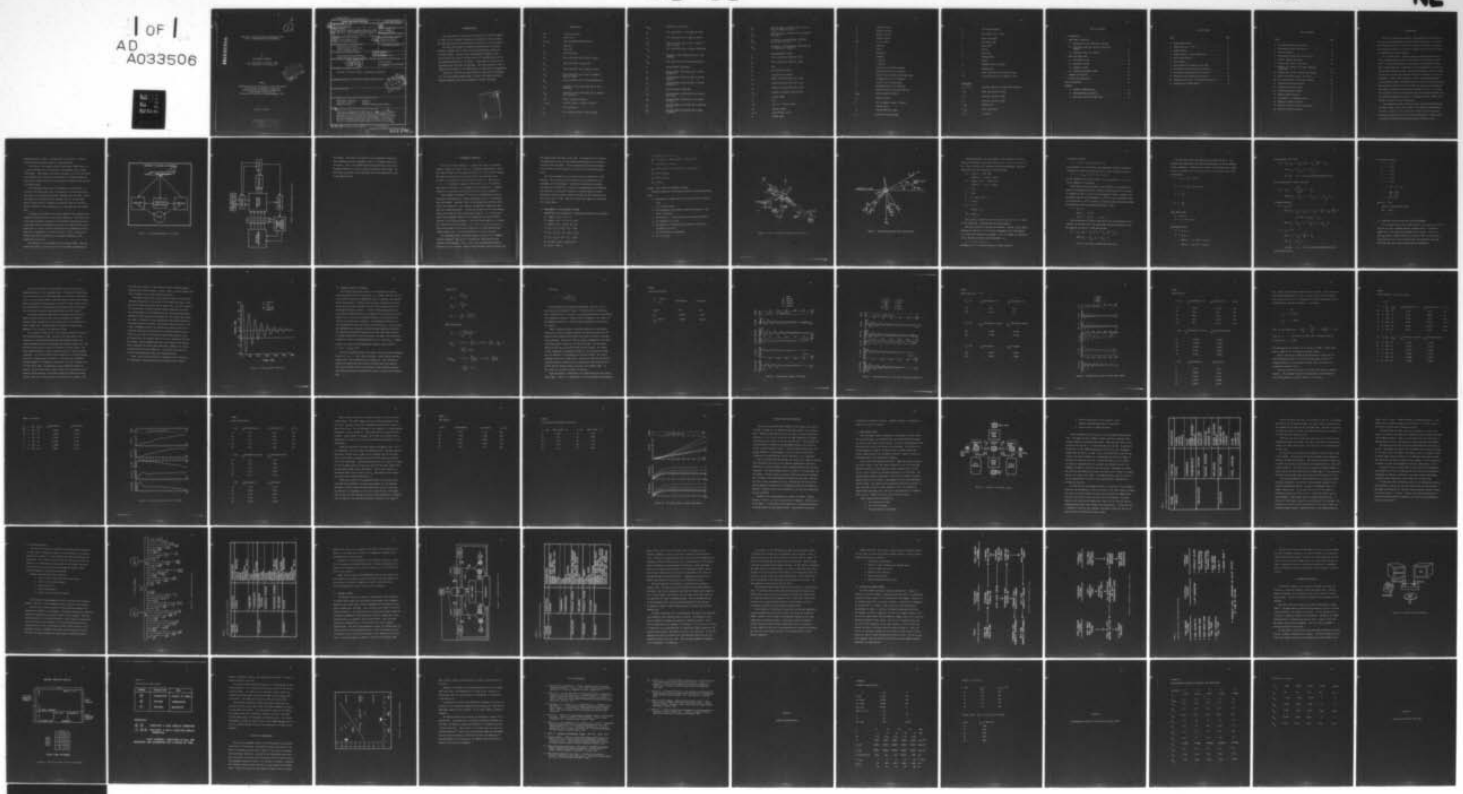

END

DATE FILMED
2-77

DESIGN OF A DIGITAL AIRCRAFT SIMULATOR FOR USE WITH A COMPUTER-AIDED DECISION-MAKER

BY

PAUL DENNIS BIOLCHINI

B.S., University of Illinois, 1974
A.B., University of Illinois, 1974

THESIS

Submitted in partial fulfillment of the requirements
for the degree of Master of Science in
Aeronautical and Astronautical Engineering
in the Graduate College of the
University of Illinois at Urbana-Champaign, 1976

Urbana, Illinois

Unclassified

SECURITY CLASSIFICATION OF THIS PAGE (When Data Entered)

REPORT DOCUMENTATION PAGE

READ INSTRUCTIONS BEFORE COMPLETING FORM

1. REPORT NUMBER: ARL-76-19/AFAL-76-1	2. GOVT ACCESSION NO.
3. RECIPIENT'S CATALOG NUMBER	
4. TITLE (and Subtitle): DESIGN OF A DIGITAL AIRCRAFT SIMULATOR FOR USE WITH A COMPUTER-AIDED DECISION-MAKER.	5. TYPE OF REPORT & PERIOD COVERED: Final Report.
	6. PERFORMING ORG. REPORT NUMBER
7. AUTHOR(s): Paul Dennis Biolchini	8. CONTRACT OR GRANT NUMBER(s): F33615-73-C-1238
9. PERFORMING ORGANIZATION NAME AND ADDRESS: University of Illinois, Aviation Research Laboratory, Savoy, Illinois 61874	10. PROGRAM ELEMENT, PROJECT, TASK AREA & WORK UNIT NUMBERS
11. CONTROLLING OFFICE NAME AND ADDRESS: Air Force Avionics Laboratory, Wright-Patterson AFB, OH 45433	12. REPORT DATE: 1976 13. NUMBER OF PAGES: 77
14. MONITORING AGENCY NAME & ADDRESS (if different from Controlling Office): 83p.	15. SECURITY CLASS. (of this report): Unclassified 15a. DECLASSIFICATION/DOWNGRADING SCHEDULE

16. DISTRIBUTION STATEMENT (of this Report)

Approved for public release; distribution unlimited.

17. DISTRIBUTION STATEMENT (of the abstract entered in Block 20, if different from Report)

18. SUPPLEMENTARY NOTES

19. KEY WORDS (Continue on reverse side if necessary and identify by block number)

Aerodynamic simulation	Controls
Equations of motion	Displays
Computer control	Computer-aided decision making

20. ABSTRACT (Continue on reverse side if necessary and identify by block number)

This report summarizes the work done on a study titled "Computer-Aided Decision Making for Flight Operations" conducted by the University of Illinois under Air Force Contract F33615-73-C-1238. The report describes in detail the development of equations of motions, simulated flight costs, and the results of the flight tests for a simplified computer model of a twin jet aircraft.

DD FORM 1 JAN 73 1473 EDITION OF 1 NOV 65 IS OBSOLETE

Unclassified

SECURITY CLASSIFICATION OF THIS PAGE (When Data Entered)

406174 LB

ACKNOWLEDGEMENT

The author wishes to express his appreciation to Professor Kenneth R. Sivier for his continual assistance as the author's thesis advisor. His help and criticism greatly assisted the author in this undertaking.

The author also wishes to express his appreciation to Professor Charles O. Hopkins and the staff of the Aviation Research Laboratory for their support. Special credit is due Patrick FitzHenry of ARL for his work as the head of the ARL effort for the CADM project and for his continued assistance to the author. It was under his direction and supervision that this work was performed. The author would also like to thank the other members of the CADM project for their help and suggestions.

Support for this work was made possible by the Avionics Laboratory, U.S. Air Force Systems Command under a contract (AF F33615-73-C-1238) entitled "Computer-Aided Decision-Making for Flight Operations."

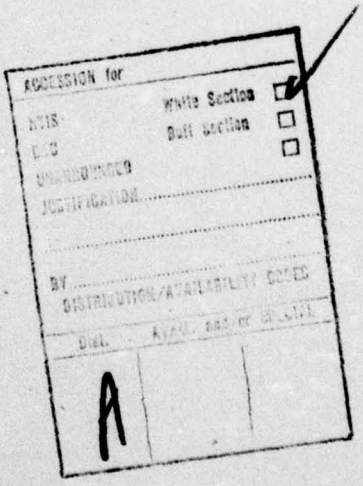

NOMENCLATURE

Alt	reference altitude
AR	aspect ratio
a_1, a_2	time non-dimensionalizing terms
b	wing span
C	side force
C_D	drag coefficient
C_{D_c}	drag coefficient due to control inputs
C_{D_o}	drag coefficient for zero lift
C_{D_α}	drag coefficient due to angle of attack
$C_{D_{\dot{\alpha}}}$	drag coefficient due to rate of change of angle of attack
$C_{D_{\delta_e}}$	drag coefficient due to elevator deflection
$C_{D_{\delta_f}}$	increment of drag coefficient due to flap extension
$C_{D_{\delta_g}}$	increment of drag coefficient due to landing gear extension
c.g.	center of gravity location
$c.g._{ref}$	reference center of gravity location
C_L	lift coefficient
C_{L_c}	lift coefficient due to control inputs

$C_{L_{max}}$	maximum lift coefficient
C_{L_o}	lift coefficient at zero angle of attack
C_{L_α}	lift coefficient due to angle of attack
$C_{L_{\dot{\alpha}}}$	lift coefficient due to rate of change of angle of attack
$C_{L_{\delta_e}}$	lift coefficient due to elevator deflection
$C_{L_{\delta_f}}$	increment in lift coefficient due to flap extension
C_{L_q}	lift coefficient due to pitching velocity
C_l	rolling moment coefficient
C_{l_c}	rolling moment coefficient due to control deflection
C_{l_p}	rolling moment coefficient due to rolling velocity
$C_{l_{\delta_a}}$	rolling moment coefficient due to aileron deflection
C_m	pitching moment coefficient
C_{m_c}	pitching moment coefficient due to control deflection
C_{m_o}	pitching moment coefficient at zero angle of attack
C_{m_q}	pitching moment coefficient due to pitching velocity
C_{m_α}	pitching moment coefficient due to angle of attack

$C_{m_{\dot{\alpha}}}$	pitching moment coefficient due to rate of change of angle of attack
$C_{m_{\delta_e}}$	pitching moment coefficient due to elevator deflection
$C_{m_{\delta_f}}$	increment in pitching moment coefficent due to flap extension
$C_{m_{\delta_g}}$	increment on pitching moment coefficent due to landing gear extension
$\bar{c}$	wing aerodynamic chord
C_x	force coefficient along the X axis
C_z	force coefficient along the Z axis
D	drag
e_o	wing efficiency factor
g	acceleration of gravity
I_x	moment of inertia about the X axis
I_y	moment of inertia about the Y axis
I_z	moment of inertia about the Z axis
I_{zx}	product of inertia in the ZX plane
L	rolling moment
L'	lift
L'_c	lift due to control inputs
M	pitching moment
m, wt	aircraft mass, weight
N	yawing moment

p	rolling velocity
q	pitching velocity
q_∞	dynamic pressure
r	yawing velocity
R/C	rate of climb
S	wing area
T	thrust
u	X velocity
V	airspeed
v	Y velocity
w	Z velocity
X	aircraft axis, positive forward
X'	aerodynamic force in X direction
Y	aircraft axis, positive along right wing
Y'	aerodynamic force in Y direction
Z	aircraft axis, positive down
Z'	aerodynamic force in Z direction
α	angle of attack of the zero-lift line
α_{abs}	absolute angle of attack
α_x	angle of attack
$\dot{\alpha}$	rate of change of angle of attack
β	sideslip angle
δ_a	aileron deflection angle
δ_e	elevator deflection angle

δ_f	flap extension angle
δ_g	gear state; 0 up, 1 down
γ	flight path angle
Λ	wing sweep angle
θ	pitch angle
ρ	density
ϕ	bank angle
ψ	heading angle
τ	period
ω_n	undamped natural frequency
ζ	damping ratio
$(\dot{})$	first derivative with respect to time
$(\ddot{})$	second derivative with respect to time

Subscripts

$(\ )_o$, $(\ )_e$	reference condition, steady-state condition
$(\ )_E$	Earth axis reference frame
$(\ )_w$	wind axis reference frame
$(\ )$	body axis reference frame
$(\ )_{ph}$	phugoid mode
$(\ )_{sp}$	short period mode
$(\ )_r$	roll mode

TABLE OF CONTENTS

LIST OF TABLES

LIST OF FIGURES

1. INTRODUCTION

In today's sophisticated aircraft, much emphasis has been placed on acquiring and displaying more and more complex information to the pilot. This trend has resulted in ever increasing pilot workloads, an undesirable situation because it increases the margin of pilot error and lowers the probability of mission success.

It is possible that a computer system can provide mathematically sound, evaluated decisions which could reduce pilot workload and pilot error.[1] The pilot then begins to function as a system manager rather than a system component. Unfortunately this reasoning does not apply to critical high workload periods. Conventional automation tends to present more data to the pilot and requires him to key in requests for specific information. Hence, while automation tends to lower workload during cruise and other similar workload periods, it tends to increase workload during critical times such as close combat or terminal area navigation.[2] Two studies of advanced cockpits and procedures by the U. S. Air Force, the Integrated Information Presentation and Control System (IIPACS)[3] and the Information Management Aspects of Integrated Avionics (IMS)[4], have tended to confirm the above predictions.

The Coordinated Science Laboratory (CSL) and the Aviation Research Laboratory (ARL), after a joint study of the IIPACS and IMS documents, feel that a solution to the problem of information overload might be found by considering systems with program intelligence. Such a system can carry out optimum decision-making tasks according to preset

guidelines under a variety of circumstances and, therefore, possibly lower workload and improve safety in flight operations.

The purpose of the Computer-Aided Decision-Maker (CADM) project is to provide documentation and techniques for developing such a program intelligence. The hardware and software developed, as well as the experience gained in the construction and operation of a prototype CADM, are being used to suggest methods of reducing pilot workload in both high and low workload areas.

An intelligent system needs an environment to interact with: to operate on and acquire data from. The purpose of the work discussed in this thesis is to provide the aircraft environment for the CADM. Figure 1 illustrates the interaction of the aircraft, the man, and the CADM. Figure 2 shows how such a computer could interact with the aircraft's systems (avionics, sensors, displays, etc.), the pilot, and the environment.

The nature of the CADM and the limits imposed by the availability of computer facilities define the form of the simulation. The necessity for a real-time aerodynamic simulation and the limited computer space available require that the aerodynamic model used be a simple one, yet not so simple that it is not a realistic reflection of the parameters that the CADM needs to manipulate in an actual aircraft. Thus, a complex aerodynamic model, while desirable for an accurate simulation, is not operationally practical.

More important to the simulation is the subsystem model. The more complex this model is, the better a test of the CADM's capabilities we

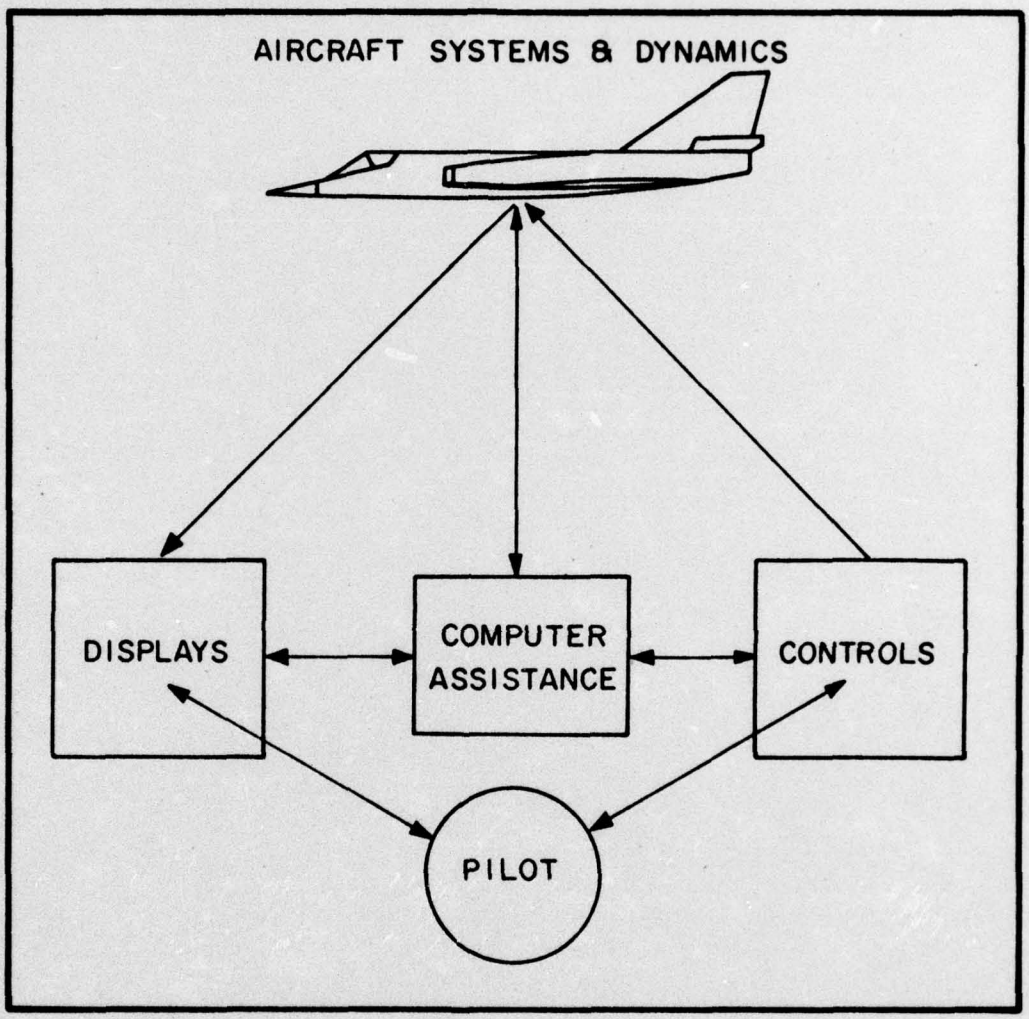

Figure 1. Aircraft/man/computer interaction.

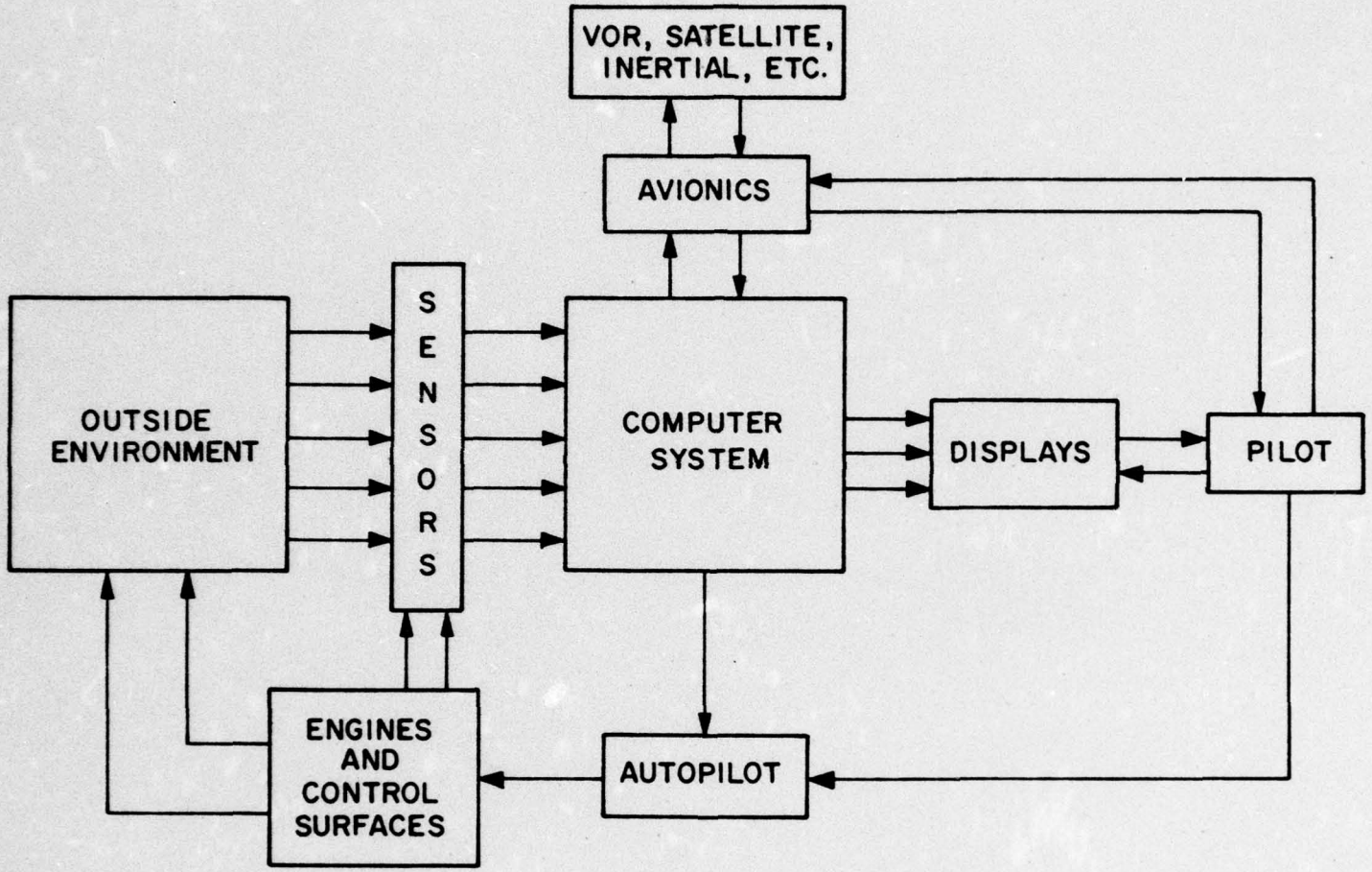

Figure 2. Systems/man/computer interaction.

can achieve. The ability of a failure in one subsystem to affect the other subsystems and the aerodynamic model is of paramount importance, not only as a test of the CADM's decision making abilities, but also in testing the ability of a pilot to work effectively with the CADM. The wide range of failures in the subsystems can tax the CADM and the pilot to any degree desired.

2. AERODYNAMIC SIMULATION

The aircraft being simulated is a single seat, twin jet, variable geometry, fighter aircraft.[5] The engines develop 15,000 pounds of thrust each and the wings have five sweep setting; 15, 25, 35, 50, and 70 degrees. The flaps are located on the trailing edges of the wings and can be extended to four positions; 10, 20, 30, and 40 degrees. The flaps can be extended for wing sweep angles of 35^{o} and less, only. The landing gear have two positions; fully extended and fully retracted. A complete listing of the aircraft's characteristics can be found in Appendix 1.

Using standard techniques,[6,7] as well as non-dimensional stability derivative representation of a high performance aircraft, an aerodynamic model was derived. Appendix 2 lists the non-dimensional stability derivatives and coefficients used. However, two important changes were made from the standard development. Lateral motion was reduced to the simplest motion; roll being the only lateral motion allowed. This not only simplified the aerodynamic model but also eliminated the need for rudder controls in the simulator hardware. The other change made was to consider only those derivatives that have a major effect on aircraft stability. The resulting model is both simple enough for real-time simulation and complex enough to be a realistic simulation of an actual aircraft.

The aerodynamic model simulation program is written in the FORTRAN computer language.[8] The program flow begins by initializing all the variables in the program. At this point, the non-dimensional stability derivatives are set to zero. After all the variables have been initialized,

the program checks the angle of the wing. The program flow is routed to the appropriate section of the program containing the initial variable values for that wing angle. The non-dimensional stability derivatives are initialized to their particular values for the current wing sweep angle.

The first variables to be calculated are the coefficients of lift and drag. The second task of the program is the calculation of the aerodynamic forces and moments. Body-axis accelerations and angular velocities are computed next. Finally, by integrating the accelerations and velocities, the body-axis velocities and Euler angles are found. Altitude is calculated from an initial altitude and the integration over time of the rate of climb. Velocity and the Euler angles are calculated in a similar manner.

2.1 DEVELOPMENT OF THE EQUATIONS OF MOTION

Etkin[6] gives the following set of equations of motion for an aircraft.

$$X' - mg\sin\theta = m(\dot{u} + qw - rv)$$

$$Y' + mg\cos\theta\sin\phi = m(\dot{v} + ru - pw)$$

$$Z' + mg\cos\theta\cos\phi = m(\dot{w} + pv - qu)$$

$$L = I_x\dot{p} - I_{zx}(\dot{r} + pq) - (I_y - I_z)qr$$

$$M = I_y\dot{q} - I_{zx}(r^2 - p^2) - (I_z - I_x)rp$$

$$N = I_z\dot{r} - I_{zx}(\dot{p} - qr) - (I_x - I_y)pq$$

$$\dot{\phi} = p + q\sin\phi\tan\theta + r\cos\phi\tan\theta$$

$$\dot{\theta} = q\cos\phi - r\sin\phi$$

$$\dot{\psi} = (q\sin\phi + r\cos\phi)\sec\theta$$

$$\dot{\alpha}_x = q - q_w \sec\beta - p\cos\alpha_x \tan\beta - r\sin\alpha_x \tan\beta$$

$$\dot{\beta} = r_w + p\sin\alpha_x - r\cos\alpha_x$$

$$p_w = p\cos\alpha_x \cos\beta + (q - \dot{\alpha}_x)\sin\beta + r\sin\alpha_x \cos\beta$$

$$\dot{x}_E = V\cos\theta_w \cos\phi_w$$

$$\dot{y}_E = V\cos\theta_w \sin\phi_w$$

$$\dot{z}_E = -V\sin\theta_w$$

Figures 3 and 4 define the geometry involved.

The above equations were developed using the following approximations:

1. The Earth is a sphere rotating on an axis fixed in inertial space
2. g is a radial vector
3. The centripetal acceleration caused by the rotation of the Earth is neglected
4. The aircraft is a rigid body and has a plane of symmetry
5. The atmosphere is at rest
6. The surface of the Earth directly under the aircraft is considered to be flat
7. All rotor effects are neglected
8. g is a constant.

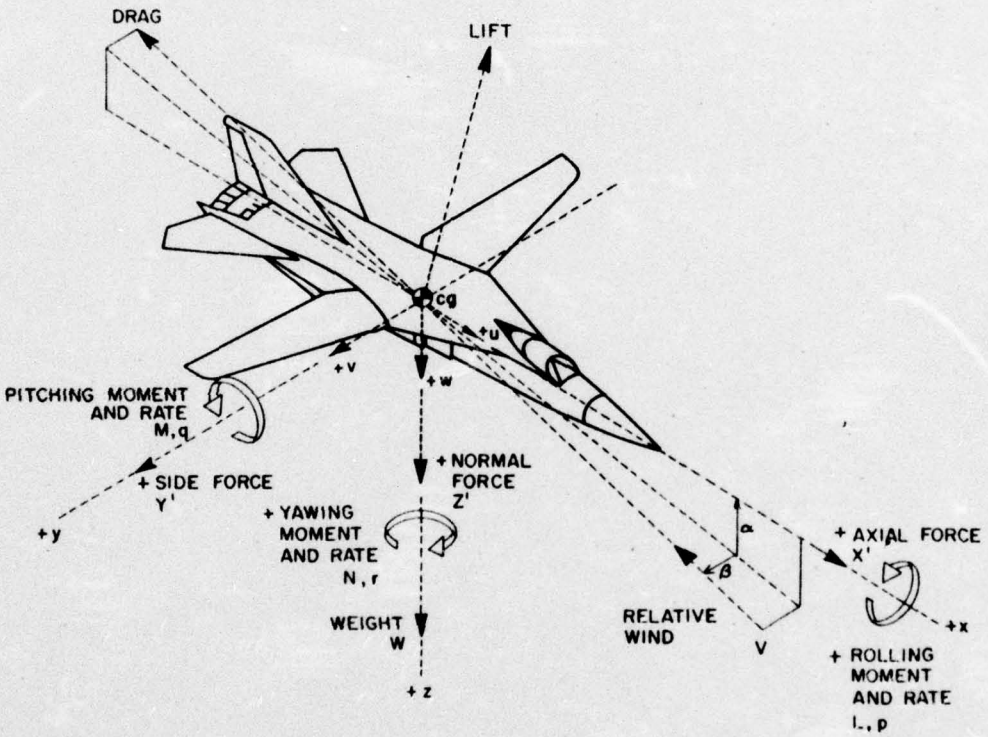

Figure 3. Aircraft geometry (adapted from Reference 7).

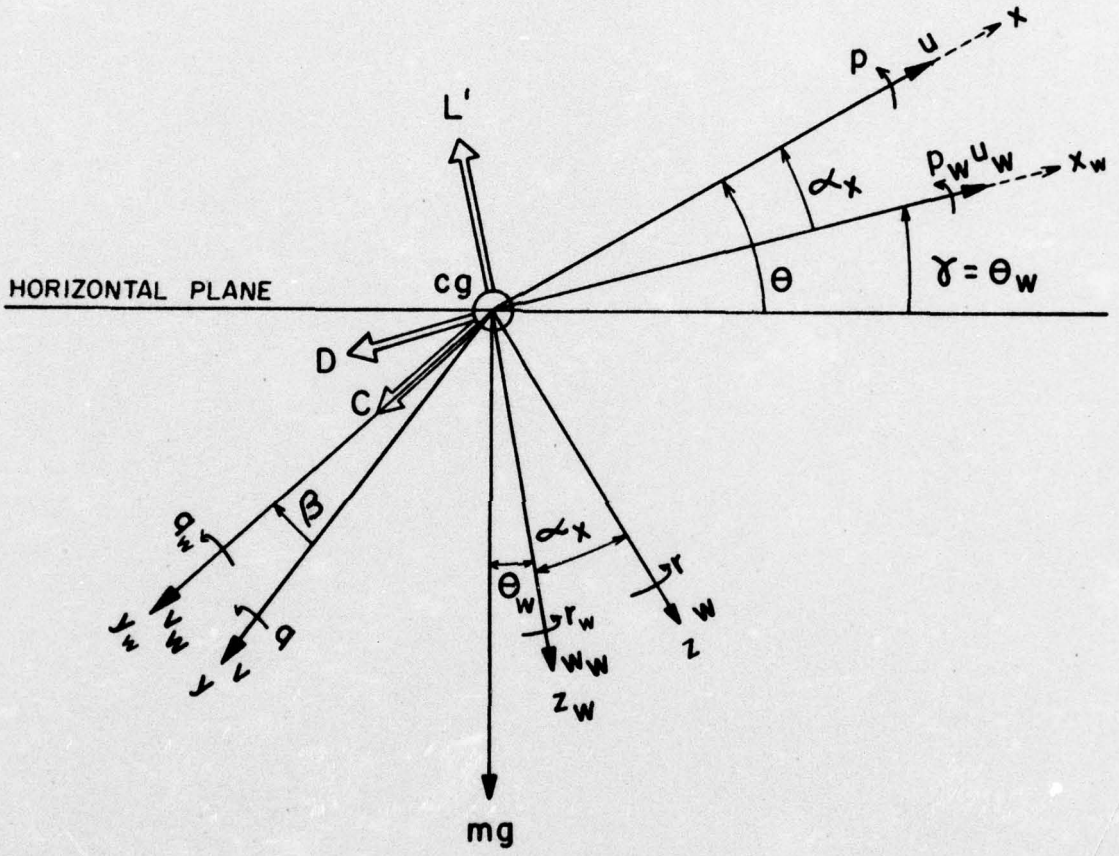

Figure 4. Relationship between body and wind axes.

As explained above, for the purposes of the simulation, lateral motion is restricted to roll motion only, e.g., $v = 0$, $\psi = \dot{\psi} = 0$, $\beta = 0$, etc. Thus, the Dutch roll and spiral modes are suppressed. With this restriction, the above equations of motion become:

$$X' - mg\sin\theta = m(\dot{u} + qw)$$

where $X' = L'\sin\alpha - D\cos\alpha$

$$Z' - mg\cos\theta\cos\phi = m(\dot{w} - qu)$$

where $Z' = -L'\cos\alpha - D\sin\alpha$

$$L = I_x\dot{p}$$

$$M = I_y\dot{q}$$

$$\dot{\phi} = p + q\sin\phi\tan\theta$$

$$\dot{\theta} = q\cos\phi$$

$$\dot{\alpha}_x = q - \dot{\gamma}$$

where $\dot{\gamma} = q_w$

$$p_w = p\cos\alpha_x$$

The $\dot{x}_E$ and $\dot{z}_E$ equations have been dropped since they are not needed for the simulation. Principal axes have been assumed.

The above equations of motion are nonlinear. However, linear approximations are used for to calculate the aerodynamic forces and moments, i.e., linear air reactions are assumed. Lift, for example, is considered to be a function of various other variables, i.e.,

$$L' = f(\alpha, \dot{\alpha}, q, L'_c)$$

Assuming that L' is a linear function of these variables,

the equation becomes:

$$L' = f_1(\alpha) + f_2(\dot{\alpha}) + f_3(q) + \Delta L'_c .$$

The individual f's are defined as the dimensional stability derivatives. Inserting the stability derivatives into the above equation we obtain:

$$L' = L'_{\alpha}\ \alpha_{abs} + L'_{\dot{\alpha}}\ \dot{\alpha} + L'_{q}\ q + \Delta L'_{c}$$

All the components of the aerodynamic forces and moments, X', Z', M, L, can be expanded in this manner.

The stability derivative data for the aircraft to be simulated are given in non-dimensional form.[5] Therefore, these data must be converted to dimensional form to be used in the equations of motion. However, the aerodynamic moments are proportional to $\rho V^2 l^3$, and the aerodynamic forces are proportional to $\rho V^2 l^2$, allowing a relatively simple conversion between the dimensional and non-dimensional equations. Thus,

$$X' = C_x q_{\infty} S$$

where $q_{\infty} = \frac{1}{2} \rho V^2$

and $C_x = C_L \sin\alpha - C_D \cos\alpha$.

The non-dimensional stability derivatives can, with appropriate conversions, be substituted for the dimensional stability derivatives, e.g., the equation for the lift coefficient becomes

$$C_L = C_{L_{\alpha}}\ \alpha_{abs} + C_{L_{\dot{\alpha}}}\ \dot{\alpha}\ a_1 + C_{L_q}\ q a_1 + C_{L_c}$$

where $C_{L_c} = C_{L_{\delta_e}}\ \delta_e + C_{L_{\delta_f}}\ \delta_f$

and a_1 is the time non-dimensionalizing term.

The equations used in the simulation are summarized below. The equations are dimensional with linear approximations for the aerodynamic forces and moments. Because of the omission of speed derivatives, proper control and dynamics will not be simulated in the transonic speed range.

Accelerations

$$\dot{u} = -wq + \frac{X}{m} - g\sin\theta$$

$$\dot{w} = uq + \frac{Z}{m} + g\cos\theta\cos\phi$$

$$\dot{p} = \frac{L}{I_x}$$

$$\dot{q} = \frac{M}{I_y}$$

Euler Angle Rates

$$\dot{\theta} = q\cos\phi$$

$$\dot{\phi} = p - q\sin\phi\tan\theta$$

Aerodynamic Forces

$$X' = C_x q_\infty S$$

$$Z' = C_z q_\infty S$$

where $C_x = C_L \sin\alpha - C_D \cos\alpha$

and $C_Z = -C_L \cos\alpha - C_D \sin\alpha$

Lift and Drag Coefficients

$$C_L = C_{L_\alpha}\ \alpha_{abs} + C_{L_{\dot\alpha}}\ \dot\alpha\ \frac{\bar c}{2V} + C_{L_q}\ \frac{q\,\bar c}{2V} + C_{L_c}$$

where $C_{L_c} = C_{L_{\delta_e}}\ \delta_e + C_{L_{\delta_f}}\ \delta_f$

and $\frac{\bar c}{2V} = a_1$, the time non-dimensionalizing term

for translational or linear velocities.

$$C_D = C_{D_0} + \frac{C_L^{\,2}}{\pi\, e_0\, AR} + C_{D_c}$$

where $C_{D_c} = C_{D_{\delta_e}}\ \delta_e + C_{D_{\delta_f}}\ \delta_f + C_{D_{\delta_g}}\ \delta_g$.

Aerodynamic Moments

$$M = C_m\, q_\infty\, S\bar c$$

where $C_m = C_{m_o} + C_{m_\alpha}\ \alpha + C_{m_{\dot\alpha}}\ \dot\alpha\ \frac{\bar c}{2V} + C_{m_q}\ \frac{q\,\bar c}{2V} + C_L\ (c.g. - c.g._{ref}) + C_{m_c}$

and $C_{m_c} = C_{m_{\delta_e}}\ \delta_e + C_{m_{\delta_f}}\ \delta_f + C_{m_{\delta_g}}\ \delta_g$

$$L = C_l\, q_\infty\, S\, b$$

where $C_l = C_{l_p}\ p\,\frac{b}{2V} + C_{l_c}$

and $C_{l_c} = C_{l_{\delta_a}}\ \delta_e$

and $\frac{b}{2V} = a_2$, the time non-dimensionalizing term for the rolling velocity.

Velocities and Angles

$$u = \int \dot{u}\, dt$$

$$w = \int \dot{w}\, dt$$

$$q = \int \dot{q}\, dt$$

$$p = \int \dot{p}\, dt$$

$$\theta = \int \dot{\theta}\, dt$$

$$\phi = \int \dot{\phi}\, dt$$

$$\alpha = \tan^{-1} \frac{w}{u} \doteq \frac{w}{u}$$

$$\dot{\alpha} = \frac{\dot{u}w - w\dot{u}}{u^2 + w^2}$$

$$V = \sqrt{u^2 + w^2}$$

Mach no. = V/A

where A is the speed of sound

$$R/C = V \sin \gamma$$

$$\gamma = \theta - \alpha$$

2.2 SIMULATED FLIGHT TEST AND DATA COLLECTION METHODS

The aerodynamic model of the CADM simulator served mainly as a side task for the pilot; applying various workloads on him. A simulated flight test of the model was performed for two reasons. First, the test was used to determine that the aerodynamic model was responding to control inputs as an actual aircraft would, and second, by analizing the flight test data, handling qualities were determined.

The stick-fixed flight test method[9] was chosen to evaluate the handling qualities of the aerodynamic model. Although this method does not exactly duplicate the flying qualities of an aircraft controlled by a pilot, the stick-fixed modes of aircraft motion are often used as parameters in specifying flying qualities criteria.[10] Thus, through the use of controlled tests, we obtained data that could be used to determine how the aircraft simulator would respond under a pilot's control.

Although the simplification of the aerodynamic model reduced the number of stick-fixed modes that could be evaluated, the number of possible flight configurations to be tested, due to the inclusion of flaps, landing gear, and wing sweep in the model, was quite large. Appendix 3 is a listing of the conditions tested.

The aerodynamic model was run on the Digital Equipment Corporation PDP 11/40 mini-computer at ARL. Because of the limitations in the computer data collection procedures and data plotting routines, two separate methods were used in performing the simulated flight test. One method was used solely to observe the effects of control inputs. The other method was used to collect quantitative data for selected flight conditions. In the first method, control inputs were initiated through the use of a plasma screen touch panel. This panel also included an attitude indicator, and numerical readouts for velocity, altitude, rate of climb, pitch angle, and bank angle, giving immediate feedback of results. In the second method, control inputs were initiated from the computer console keyboard. Using these inputs, the simulator program was run. Data were collected from it and stored in the computer. The

data were then output to a line printer through a plotting program. Numerical data were also output. Figure 5 shows a typical computer plot. Every variable in each condition had its own plot.

The control inputs were a -.02 radian step input to the elevator (forcing the aircraft's nose up) and a +.175 radian step input to the ailerons (forcing the aircraft into a right roll). For each condition, the controls were activated when the simulator program was started. The starting point for the simulator was the calculated steady-state condition for that particular configuration. Two testing time periods were used: 20 seconds for short period mode data and 480 seconds for the phugoid and roll mode data. The initial flight condition for the "clean" configuration was at the steady-state values of the rate of climb and climb angle associated with an altitude of 5000 feet and a velocity of as close to 450 feet per second as was practical, with the exception of one condition that was run at a velocity of 300 feet per second. Flap and landing gear tests were started at the steady-state conditions for various other velocities. However, the initial altitude for all tests was 5000 feet. The initial velocities are listed on the appropriate tables presenting these data.

Note: The initial velocities (V_e) presented in the tables are the equilibrium velocities before the deflection of the controls.

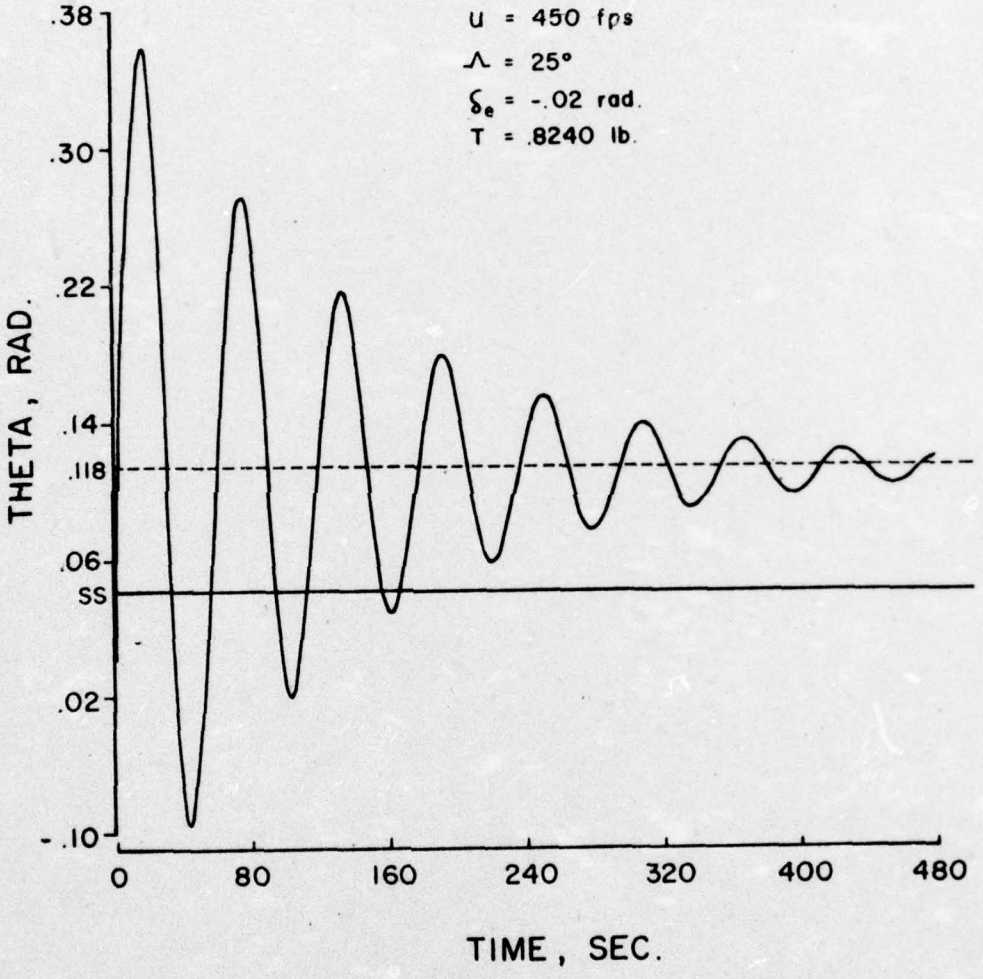

Figure 5. Typical computer data plot.

2.3 SIMULATED FLIGHT TEST RESULTS

The 25^{o} wing sweep angle was the only configuration for which complete graphical data were collected, i.e., flight tests were run for every possible flap angle, landing gear and c.g. position, and aircraft weight configuration. Graphical data were also collected for elevator and aileron step input responses for the "clean" configuration of the remaining wing sweep positions. A "clean" configuration meant that the flaps and landing gear were not extended, the aircraft was at gross weight, the c.g. was at the reference position, and the aircraft was flying in the steady-state condition. The remaining conditions were run and observed on the plasma panel attitude indicator. Here, stability was confirmed if no divergence occurred and some damping was observed. All conditions tested were observed to be stable under these criteria. It should be noted that because no provision was made in the simulation program for a direct relationship between the c.g. and the $C_{m_{\alpha}}$, changes in the c.g. affected the pitching moment equation only through the C_L (c.g. - c.g._{ref}) term.

Before the simulated flight tests began, the basic dynamic characteristics, i.e., ω_n, ζ, and τ were calculated. These results were then compared with those determined in the flight test. Some differences between the experimental data and the calculated data were expected since the predicted results were calculated using approximate methods. The following equations from Etkin[6] were used to calculate the predicted data.

Phugoid Mode:

$$\tau_{ph} = \frac{\pi \sqrt{2}\ V_e}{g}$$

$$\omega_{n_{ph}} = \frac{\sqrt{2}\ g}{V_e}$$

$$\zeta_{ph} = \frac{1}{\sqrt{2}} \left(\frac{D}{L'} \right)_e$$

Short Period Mode:

$$\tau_{sp} = \frac{2\pi}{\omega_{n_{sp}} \sqrt{1 - \zeta_{sp}^2}}$$

$$\omega_{n_{sp}}^2 = -\left(q_\infty S \bar{c}\ \frac{C_{m_\alpha}}{I_y} + \left(q_\infty S \bar{c}\ \frac{C_{m_q}}{I_y}\ \frac{\bar{c}}{2V_e} \right) \cdot \left(\frac{q_\infty S}{m V_e}\ C_{L_\alpha} \right) \right)$$

$$2\zeta_{sp}\omega_{n_{sp}} = -\left(q_\infty S \bar{c}\ \frac{C_{m_{\dot{\alpha}}}\ \bar{c}}{I_y\ 2V_e} + q_\infty S \bar{c}\ \frac{C_{m_q}\ \bar{c}}{I_y\ 2V_e} - \frac{q_\infty S}{m V_e}\ C_{L_\alpha} \right)$$

Roll Mode:

$$\tau_r = \frac{4 I_x}{(\rho S b^2 V_e C_{l_p})}$$

The experimental and predicted phugoid mode data for the 25^o sweep angle are presented in Table 1. The data show very good agreement, indicating that, at least for the long period motions, the simulator is performing as expected. Figure 6 gives an example of the output for the phugoid mode motions. The short period response has been omitted for clarity.

Figure 7 shows the effect of elevator deflection on equilibrium flight for two initial flight conditions, one well above the speed for minimum thrust required and the other just below the speed for minimum thrust required. For the 25^o wing sweep angle configuration, the speed for minimum thrust required is 317 feet per second. The two speeds chosen are 450 feet per second and 300 feet per second. The results of this comparison are presented in Table 2. The graphical data show that the simulator is performing as an aircraft should. The α and q variables settle to the same points. The rate of climb for the 450 fps condition shows an increase from the steady-state value while the R/C for the 300 fps condition shows a decrease, even though slight. In both cases, the airspeed decreases as expected.

Figure 8 presents a comparison of the phugoid mode data for various sweep angles. Table 3 is a presentation of the experimental and predicted

TABLE 1

Phugoid Mode Results

$V_e = 450$ fps, $\Lambda = 25^o$	Experimental	Calculated
τ_{ph}, sec	59.5	62.1
ζ_{ph}	0.0918	0.106
$\omega_{n_{ph}}$, rad/sec	0.1058	0.1012

T = 8240
V_e = 450 fps
α_e = .066 rad
θ_e = .045 rad
n = 5000 ft.

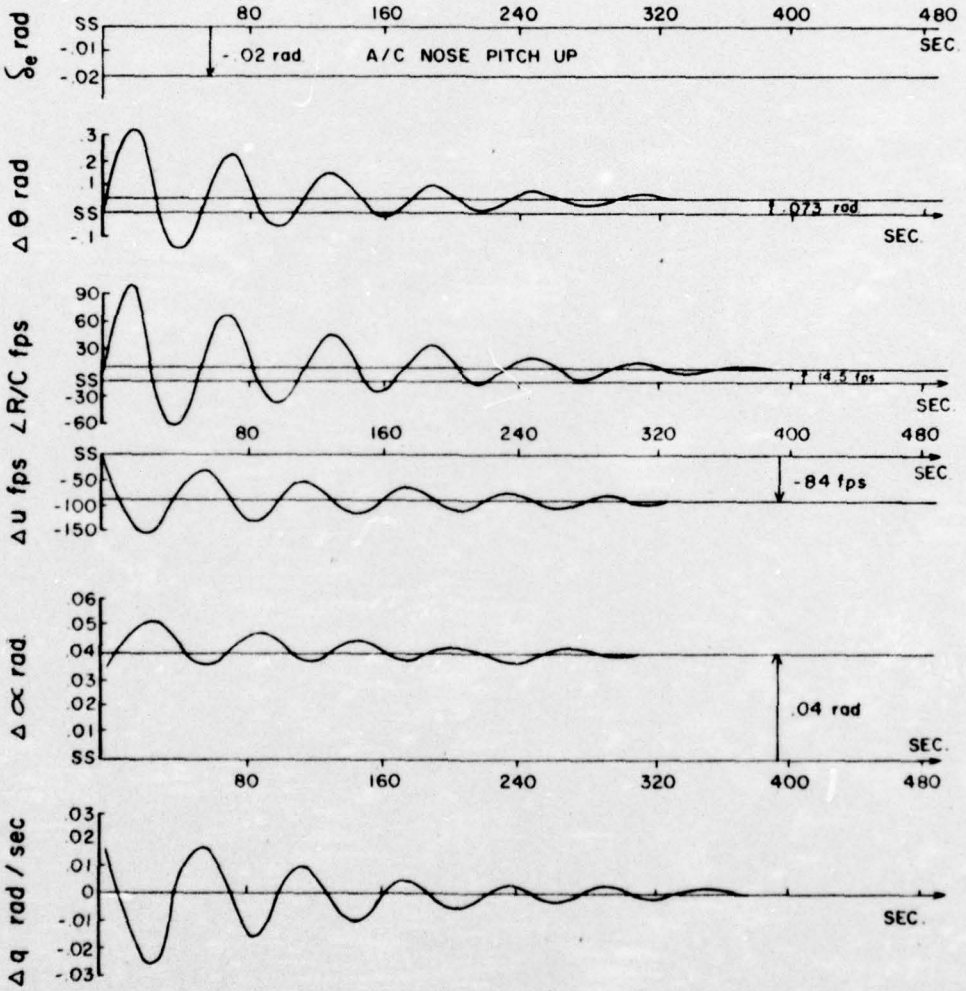

Figure 6. Phugoid mode results, 25° sweep.

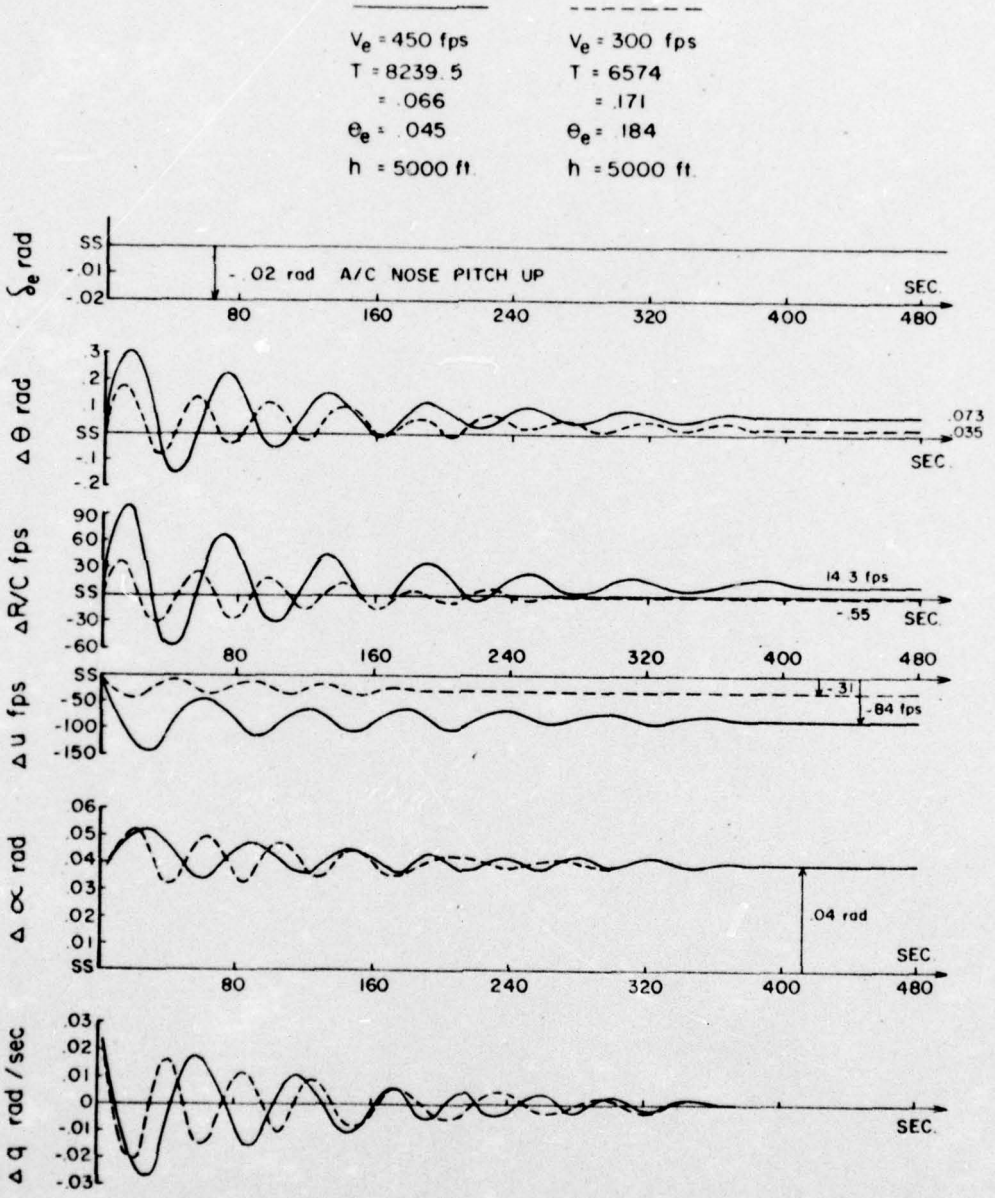

Figure 7. Phugoid mode results, 25° sweep, different velocities.

TABLE 2

Phugoid Results, $\Lambda = 25^{o}$

V_e, fps	τ_{ph} Experimental, sec	τ_{ph} Calculated, sec
450	59.5	62.1
300	41.92	41.4

V_e, fps	$\omega_{n_{ph}}$ Experimental, rad/sec	$\omega_{n_{ph}}$ Calculated, rad/sec
450	0.1058	0.1012
300	0.1502	0.1518

V_e, fps	ζ_{ph} Experimental	ζ_{ph} Calculated
450	0.0918	0.106
300	0.0664	0.0845

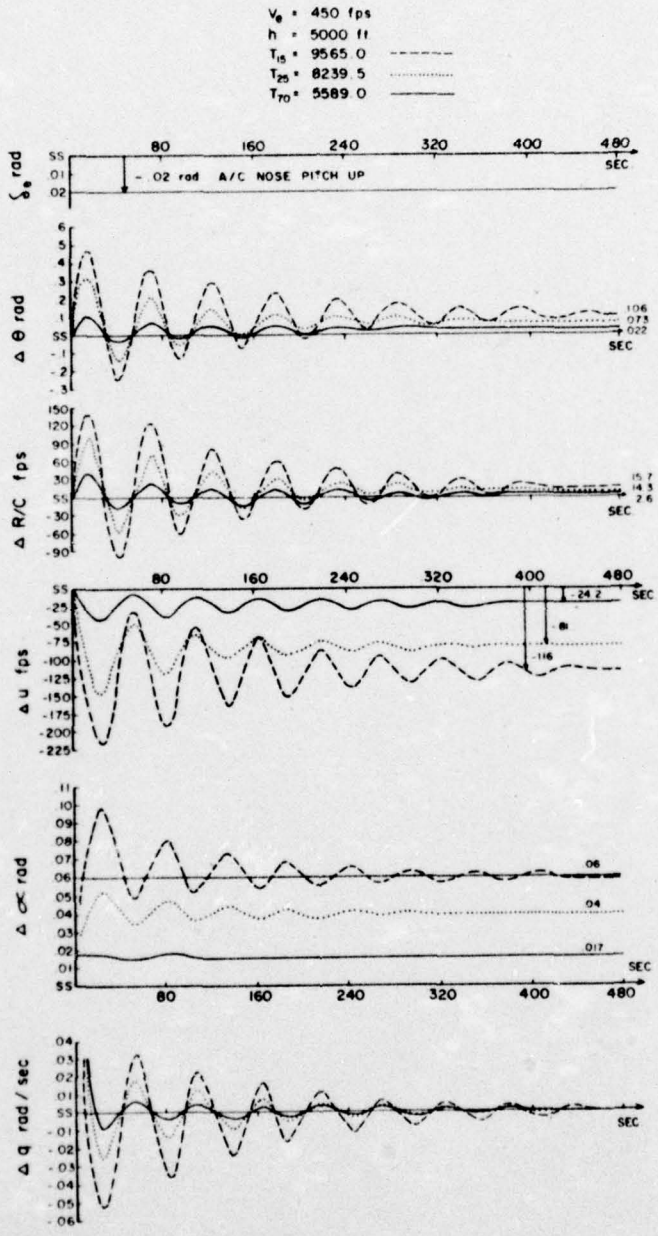

Figure 8. Phugoid mode results, various sweep angles.

TABLE 3

Phugoid Results

Λ, deg	τ_{ph} Experimental, sec	τ_{ph} Calculated, sec.	V_e, fps
15	58.56	61.69	447
25	59.5	62.1	450
35	60.8	61.69	447
50	60.4	61.41	445
70	60.4	61.27	444

Λ, deg	$\omega_{n_{ph}}$ Experimental, rad/sec	$\omega_{n_{ph}}$ Calculated, rad/sec
15	0.1079	0.1018
25	0.1058	0.1012
35	0.1041	0.1018
50	0.1042	0.1023
70	0.1041	0.1025

Λ, deg	ζ_{ph} Experimental	ζ_{ph} Calculated
15	0.107	0.123
25	0.0918	0.106
35	0.0872	0.106
50	0.0656	0.0889
70	0.0511	0.0719

data. Again, good agreement between the two is shown. In all cases, the phase relationships between θ and α, θ and q, and θ and u are correct. Also, the final values of α correspond to the values calculated from the non-dimensional stability derivatives. For example,

$$\Lambda = 25^{o}$$

$$C_{m_{\delta_e}} = -1.6/\text{rad}$$

$$C_{m_{\alpha}} = -.8/\text{rad}$$

where, in the steady-state $\frac{\Delta \alpha}{\Delta \delta_e} = \frac{C_{m_{\delta_e}}}{C_{m_{\alpha}}} = \frac{-(-1.6)}{-.8} = -2.0$

thus, if $\delta_e = -.02$ rad or (-1.144^{o}), the α increase should be

$(-1.144)\ (-2.) = 2.288^{o}$

The experimental data yields a $\Delta\alpha$ of .04 rad or 2.288^{o}. Similar agreement is shown for all the phugoid conditions tested.

Table 4 presents the predicted and experimental results for the other conditions tested for the 25^{o} wing sweep angle. Because no unexpected motions or data appeared in these tests, the data is not presented in graphical form.

The short period mode results for the 25^{o} sweep angle are shown in Figure 9. The agreement between the experimental and predicted data for all wing angles, as shown in Table 5, is very good.

TABLE 4

Phugoid Results, Various Conditions

$\Lambda = 25^{o}$

δ_f	δ_g	wt, lb	c.g., chord	τ_{ph} Experimental, sec	τ_{ph} Calculated, sec	V_e, fps
20	0	55K	.35	45.76	43.61	316
40	0	55K	.35	51.52	50.65	367
0	1	55K	.35	59.84	61.65	446.7
0	0	35K	.35	58.24	61.93	448.75
0	0	55K	.30	60.48	61.63	446.6
0	0	55K	.40	59.20	61.96	449.1

δ_f	δ_g	wt, lb	c.g., chord	$\omega_{n_{ph}}$ Experimental, rad/sec	$\omega_{n_{ph}}$ Calculated, rad/sec
20	0	55K	.35	0.1377	0.1441
40	0	55K	.35	0.1223	0.1241
0	1	55K	.35	0.1027	0.1019
0	0	35K	.35	0.1018	0.1012
0	0	55K	.30	0.1002	0.1019
0	0	55K	.40	0.1005	0.1014

TABLE 4 (continued)

δ_f, deg	δ_g	wt, lb	c.g., %chord	ζ_{ph} Experimental	ζ_{ph} Calculated
20	0	55K	.35	0.0755	0.0874
40	0	55K	.35	0.0798	0.0943
0	1	55K	.35	0.1152	0.125
0	0	35K	.35	0.1329	0.147
0	0	55K	.30	0.0869	0.106
0	0	55K	.40	0.848	0.106

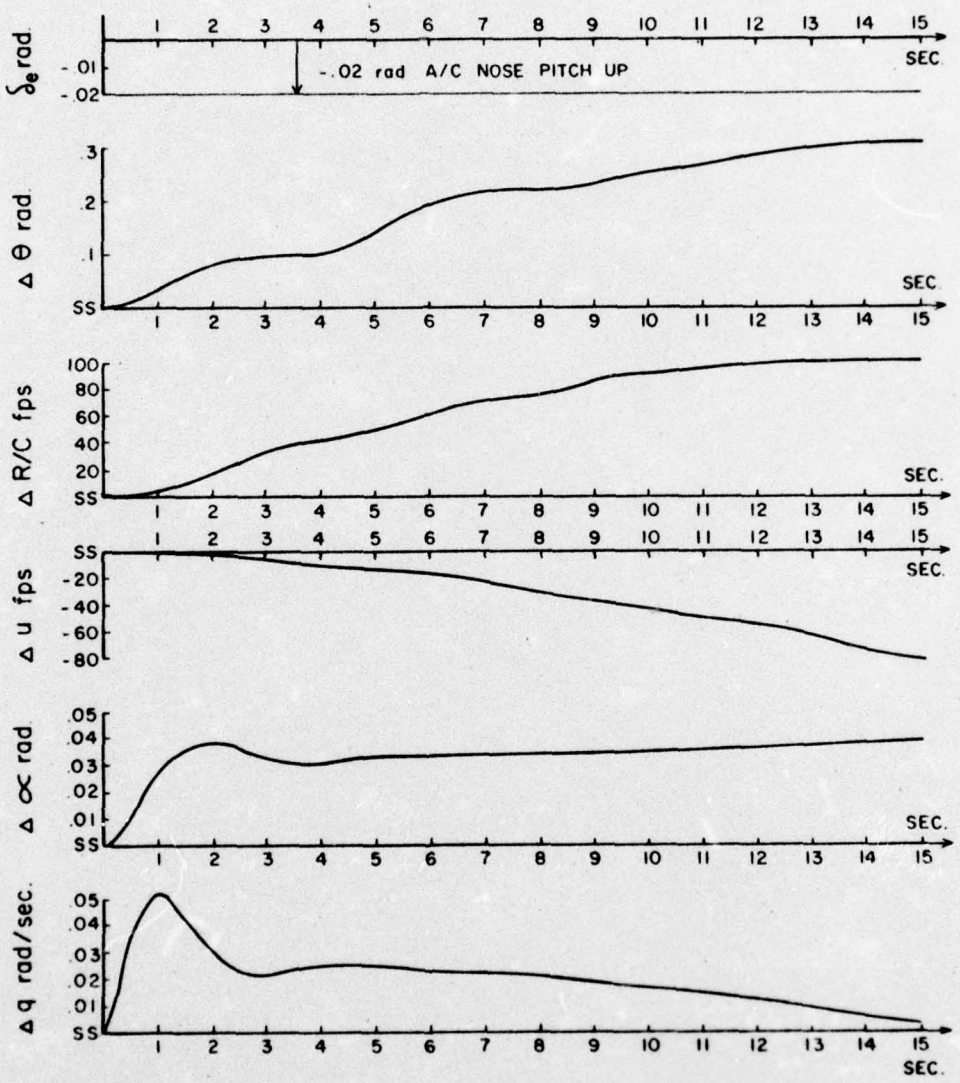

Figure 9. Short period mode results, 25° sweep.

TABLE 5

Short Period Results

Λ, deg	τ_{sp} Experimental, sec	τ_{sp} Calculated, sec	V_e fps
15	3.97	4.54	447
25	3.72	3.86	450
35	3.36	3.48	447
50	3.20	3.30	445
70	2.92	3.06	444

Λ, deg	$\omega_{n_{sp}}$ Experimental, rad/sec	$\omega_{n_{sp}}$ Calculated, rad/sec
15	1.58	1.654
25	1.79	1.897
35	1.96	2.064
50	1.96	2.050
70	2.14	2.144

Λ, deg	ζ_{sp} Experimental	ζ_{sp} Calculated
15	0.535	0.548
25	0.503	0.516
35	0.472	0.486
50	0.364	0.373
70	0.279	0.283

Table 6 gives the results of aircraft response to a +.175 rad step aileron input. This table compares the time to half amplitude for the roll mode. Agreement between the experimental and predicted results is, again, fairly good. The roll response of the simulator, a flying qualities paramenter, is given in Table 7. These data indicate a quite fast roll response. This response is, perhaps, not as fast as it should be for a fighter-type aircraft, but it is very acceptable for the purposes of the CADM project.

Figure 10 presents the roll mode results in graphical form. As is to be expected, the p and $\dot{\phi}$ data correspond very well. The most interesting result of these tests is that the roll response for the 35^{o} sweep angle is the slowest, followed by that for the 25^{o} sweep and then that for the 15^{o} sweep angle. This would indicate that roll response in cruise (25 and 35 degree angles) is lower than that for slow speed flight (15^{o}) and high speed flight (50 and 70 degrees). This is not, however, an unexpected result since the size of the C_{l_p} derivatives for the various wing sweep angles indicate this result.

Overall, the results of the simulated flight test are quite good. Predicted and experimental data show good agreement in all conditions and modes. From the results of the various tests we can be sure that the simulator is responding as an actual aircraft should. The phugoid, short period, and roll mode data also give enough information to indicate that the simulator has satisfactory handling qualities in all modes.[11]

TABLE 6

Roll Results

Λ, deg	$\tau_{1/2}$ Experimental	$\tau_{1/2}$ Calculated	V_e, fps
15	0.29	0.332	450
25	0.35	0.407	450
35	0.34	0.383	450
50	0.61	0.644	450
70	1.44	1.72	450

TABLE 7

Flying Qualities Parameters, Roll Mode

Λ, deg	Time to 30^{o}, sec	Λ, deg	Time to 60^{o}, sec
15	1.09	15	2.05
25	1.20	25	2.08
35	1.28	35	2.16
50	1.57	50	2.59
70	1.74	70	2.66

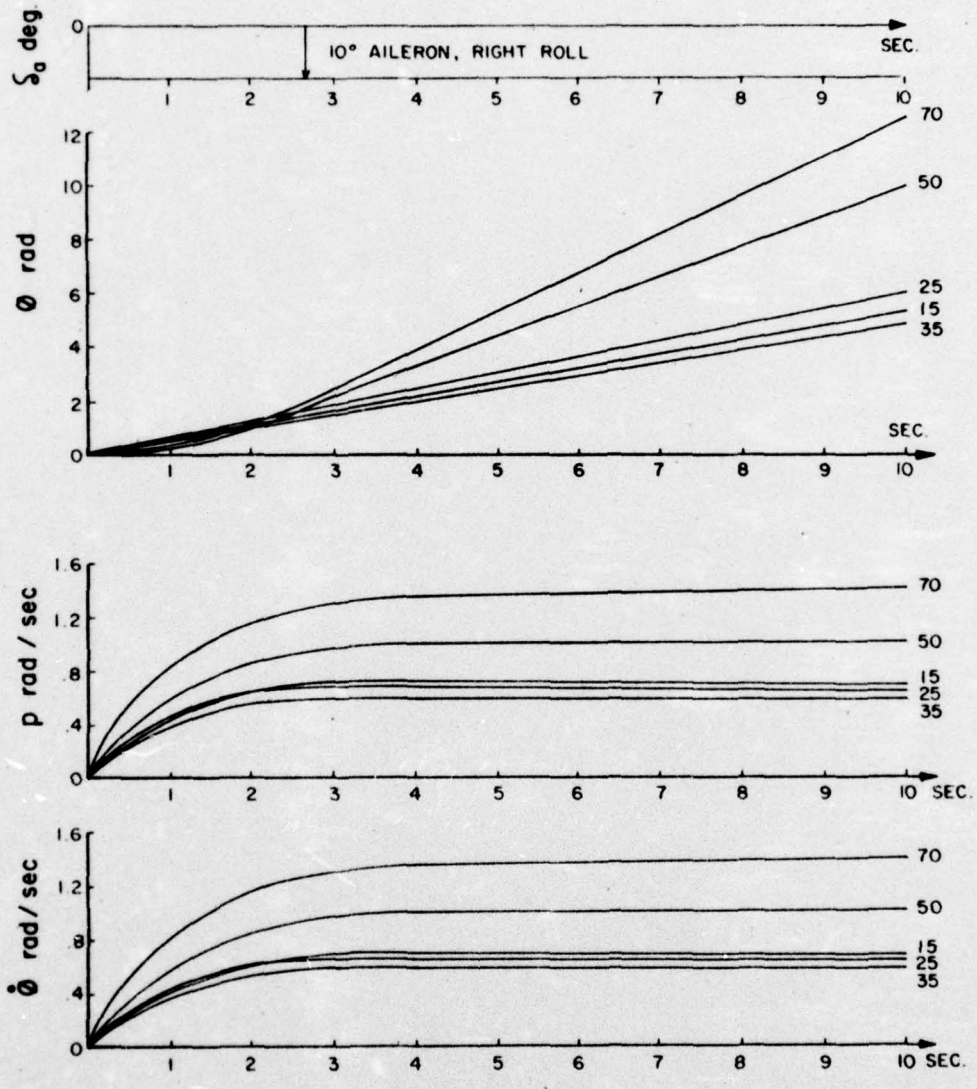

Figure 10. Roll mode results, various sweep angles.

3. AIRCRAFT SUBSYSTEM SIMULATION

The aircraft subsystem model (AIRSYS) is the primary work area for the CADM. Through it, the CADM can investigate and act on its environment. AIRSYS provides CADM with numerical data on various systems and components of the aircraft and allows the CADM alternatives in correcting failures when a system or systems malfunction(s). The aircraft subsystems modeled in AIRSYS are the Fuel/Engine System, the Electrical System, and the Hydraulic System. A central program controls the flow through AIRSYS by cycling through a series of calls to subroutines responsible for simulating the various components of the subsystems.

These particular aircraft systems were chosen for a number of reasons. Since the general task area of the CADM was degraded mode operations, AIRSYS had to simulate hardware readily identified with actual aircraft components. The chosen hardware had to be capable of failure modes, and if possible, alternate paths for failure correction had to be provided. Thus, included in the Fuel/Engine System were two fuel tanks, alternate fuel flow routes, and numerous valves. Mechanically and electrically driven pumps were provided in the Fuel/Engine System and the Hydraulic Systems. Hydraulic and electric activation of the flap and landing gear was also included.

Gremlin is the program which sets failures in AIRSYS. Through Gremlin, a failure can occur in any system or component. Failures occur on two levels. A soft failure is one which can be corrected by closing a circuit breaker or some similar action. A hard failure can not be

corrected by the CADM or the pilot. Gremlin, however, can change the status of any level of failure.

3.1 FUEL/ENGINE SYSTEM

The Fuel/Engine System is composed of two engines, two fuel tanks, two tank drain pumps, one intertank pump, two engine-driven fuel pumps, two electric fuel pumps, and four valves. The valve and plumbing network allows one fuel tank to feed either or both engines. In addition, the system produces, through the Electrical System, sensor outputs and failure characteristics for the CADM to evaluate. Figure 11 shows the interconnection of this hypothetical hardware.

Any of the system components can fail. Pumps and valves can jam in any current state. Since the center of gravity (c.g.) of the aircraft depends on whether the fuel tanks are empty, partially full, or full, the c.g. can be affected by incorrect draining of the fuel tanks. The engines produce thrust proportional to the fuel flow and the altitude. Engine failures are as follows. The engines can catch fire and produce reduced thrust. The engines can be destroyed and produce no thrust, or they can flame out with no thrust produced. Fuel flow, because of jammed valves and pumps can be cut off or continued when it is undesirable to do so. Sensors can jam or give erroneous readings.

Sensor outputs from this system are:

1. Fuel available in tanks
2. Fuel flow to engines
3. Measured thrust of each engine

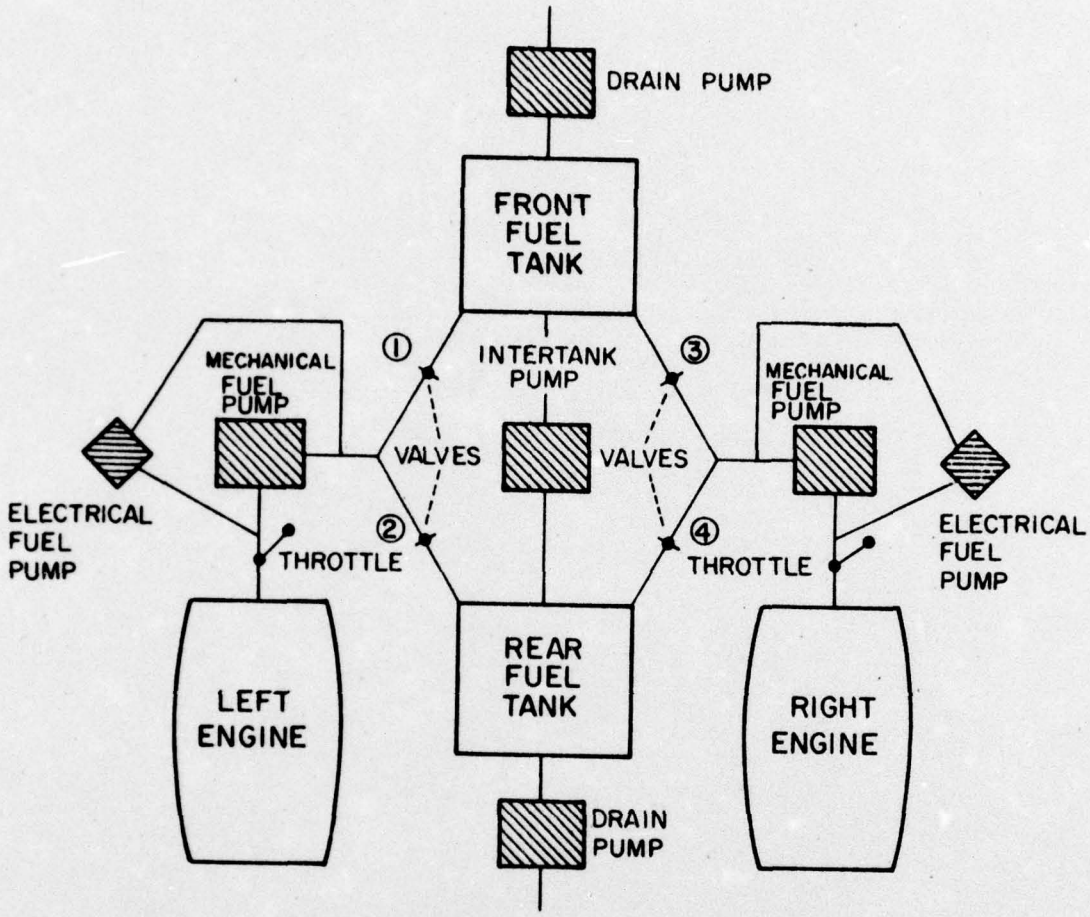

Figure 11. Simulated fuel/engine system.

4. Measured temperature of each engine's exhaust
5. Measured vibration modulation of each engine
6. Current states of pumps and valves.

Table 8 summarizes the activities of the Fuel/Engine System simulation. The CADM, the pilot, AIRSYS, Gremlin, and the aerodynamic model interact through a Shared Data Base (SDB). Each reads the data it needs and writes the results of its operation back into the SDB. The method of interaction for all AIRSYS programs and, in this case, the Fuel/Engine System, with the SDB is the same. First, the entire SDB is read and any failures specified by Gremlin are acknowledged by setting jam flags for the specific components affected. Control settings set by the CADM or the pilot are implemented if not prevented by a Gremlin set jam. For example, the CADM may ask that a valve be closed. Regardless of whether the valve has previously been closed, the valve is set "closed" if Gremlin has not set a jam of that valve. If Gremlin has set a jam, the valve can not be changed from its previous state and the CADM is informed that a failure has occurred.

The fuel flow in the plumbing network is a function of four variables. These are the availability of fuel, the state of the valves (open or closed), the state of the fuel pumps (on or off), and the amount of demand thrust. There are 156 possible routes for fuel flow in the network. The Fuel/Engine System simulation determines what amount of fuel flow the current plumbing network will allow, based on the valve states. A route for fuel is feasible if there is fuel available, the pump to force the fuel is on, and the valves controlling the path are open.

TABLE 8

Fuel/Engine System Simulation Activities

PHASE	FUNCTION	PARAMETER
INPUTS	STATES	PUMPS VALVES ENGINES
	COMMANDS	PILOT CADM
	CONSTRAINTS	OTHER SYSTEMS GREMLIN
CALCULATES	FUEL SYSTEM	DIRECTION QUANTITY
	ENGINE SYSTEM	OPERATION SENSOR DATA
	INFLUENCE	OTHER SYSTEMS GREMLIN
OUTPUTS	ENGINE SYSTEM	TEMPERATURE VIBRATION THRUST
	FUEL SYSTEM	FLOW QUANTITY LOCATION

For the intertank fuel line, the direction of the flow is determined by the state of the intertank pump. The rate of flow is either zero or the maximum rate possible for the intertank pump. The state of the pump is under the control of Gremlin, the CADM, and the pilot, or AIRSYS, if the tank auto-level function is on.

The drain fuel lines in the tanks have only one direction of flow: overboard from the source tank. The state of the pump is determined by Gremlin, the CADM, and the pilot. The flow rate is the maximum possible for the pump.

The direction of fuel flow to the engines is from the source tanks to the engines. The states of the valves and pumps are determined by Gremlin, the CADM, and the pilot. The flow rate through the engine pump is either zero or the rate specified for the demand thrust by the pilot's throttle position. The fuel flow rate through the plumbing network is either zero or the rate required by the engine pumps. If two pipes have fuel flow into the same pump, each carries half the demand fuel load.

With the preceeding fuel network description, we can now describe the engine simulation. The amount of actual thrust produced by each engine, called measured thrust, is equal to the demand thrust if no engine failures exist. If the fuel flow is zero or the engine is destroyed, the measured thrust is zero. A destroyed engine state is nonrecoverable. Only Gremlin can set an engine destroyed state. A flame out of the engine, caused by fuel starvation, is recoverable. The procedure for recovery is to re-establish fuel flow to the engine and perform an engine restart. Either the pilot or the CADM may issue an

engine restart command. AIRSYS responds by attempting ignition of the engine and resetting the engine restart function. A restart can not be initiated if the Electrical System has failed.

An engine flame out state can be set by Gremlin. To restart the engine, fuel flow to the engine is established by the previously described fuel network procedures. Thus, fuel starvation can occur from pilot or CADM blunders as well as from deliberate failure settings from Gremlin.

The measured thrust will be half the demand thrust if the engine is on fire. The engine fire state is set by Gremlin and is reset by turning off the fuel flow to the engine. The engine is now in a flame-out state. To obtain thrust again, the pilot or the CADM must start fuel flow back into the engine and issue an engine restart command. In this simulation, no penalty is given for attempting to restart an engine after a fire.

A general clean-up of state flags is performed at the beginning of every AIRSYS "write" into the SDB and specific items for which AIRSYS is responsible are updated. Examples of such items from the Fuel/Engine System are engine temperature, engine vibration, and fuel flow.

Both the pilot and the CADM have access to the information necessary and the means to correct any soft jam caused failure through the SDB. The number and complexity of failures to this particular system is large, as are the possible corrections. Through such complex manipulation of this and the other systems of AIRSYS, we can apply varying workloads to the pilot and the CADM.

3.2 ELECTRICAL SYSTEM

The Electrical System is composed of two engine driven generators, two fuel pumps, two hydraulic pumps, 48 circuit breakers, all sensors, and all valve actuators. It also includes the back-up landing gear and flap motors. Some failures in this system are caused by the incorrect opening of the individual circuit breakers for the AIRSYS components. Other failures result from the system causing the sensors to give erroneous readings to the pilot and the CADM.

Outputs from this system are as follows:

1. Status of electrical pumps, motors, and valves
2. Status of the circuit breakers
3. Status of sensors
4. Status of generators
5. Status of entire Electrical System.

The structure of the mathematical model of the Electrical System is shown in Figure 12. Table 9 summarizes the activities of this system.

The Electrical System contains two relay connected generator subsystems, one connected to each engine. An engine driven generator supplies power to a distributing bus through a master circuit breaker. Each bus distributes power to 23 AIRSYS components, each of which is connected to the bus through a circuit breaker. If one of the generators can not supply power to its bus, either through engine failure, failure of the generator itself, or jamming of the master circuit breaker in an open position, the other generator can supply power to both buses with no

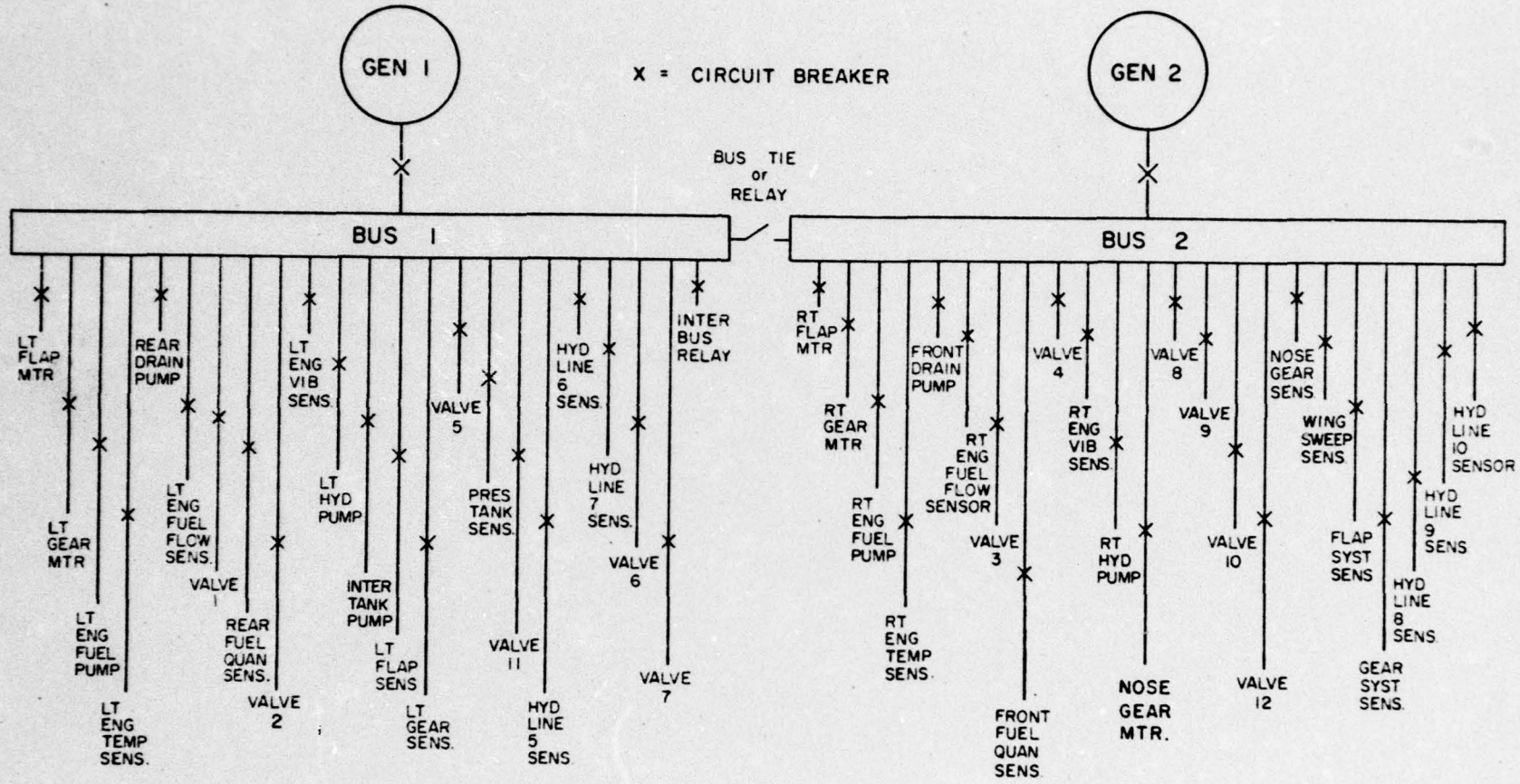

Figure 12. Simulated electrical system.

TABLE 9

Electrical System Simulation Activities

PHASE	FUNCTION	PARAMETER
INPUTS	STATES	CIRCUIT BREAKER VALVES PUMPS MOTORS GENERATORS INTERBUS RELAY
	COMMANDS	PILOT CADM
	CONSTRAINTS	GREMLIN OTHER SYSTEMS
ACTIVATES	FUEL/ENGINE SYSTEM	PUMPS VALVES SENSORS
	HYDRAULIC SYSTEM	PUMPS VALVES SENSORS MOTORS
	ELECTRICAL SYSTEM	INTERBUS RELAY CIRCUIT BREAKERS
	INFLUENCE	GREMLIN OTHER SYSTEMS
OUTPUTS	STATES	CIRCUIT BREAKERS VALVES PUMPS MOTORS GENERATORS INTERBUS RELAY

reduction in current to any component, but only if the interbus relay is closed. If the relay will not close, the components connected to the failed generator's bus will fail.

Failure of the entire Electrical System results in the loss of most of the components in the AIRSYS simulation. However, depending on the status of the components at the time of failure, such a loss need not be fatal to the aircraft.

Again, both the pilot and the CADM have access to all outputs from this system, and the means to correct any failure with the exception of one caused by a hard jam. Gremlin has access to all parts of the Electrical System and can set failures in any component.

3.3 HYDRAULIC SYSTEM

The Hydraulic System is composed of one hydraulic fluid reservoir, two engine driven pumps, two electrically driven pumps, one accumulator pressure tank, eight valves, and the mechanisms for activating the wing sweep, landing gear, and flaps. The structure of the Hydraulic System is shown in Figure 13. The activities of this system are listed in Table 10. Failures of components in this system can cause the landing gear, flaps, and wing sweep to be jammed in their current states. Also, the wing sweep can be jammed because of reduced pressure in the accumulator pressure tank. Even with reduced pressure, however, the landing gear and flaps can still be operated hydraulically. Leaks can develop in any of the hydraulic lines, forcing the shut-down of the components fed by that line. A leak also reduces the amount of fluid in the reservoir tank.

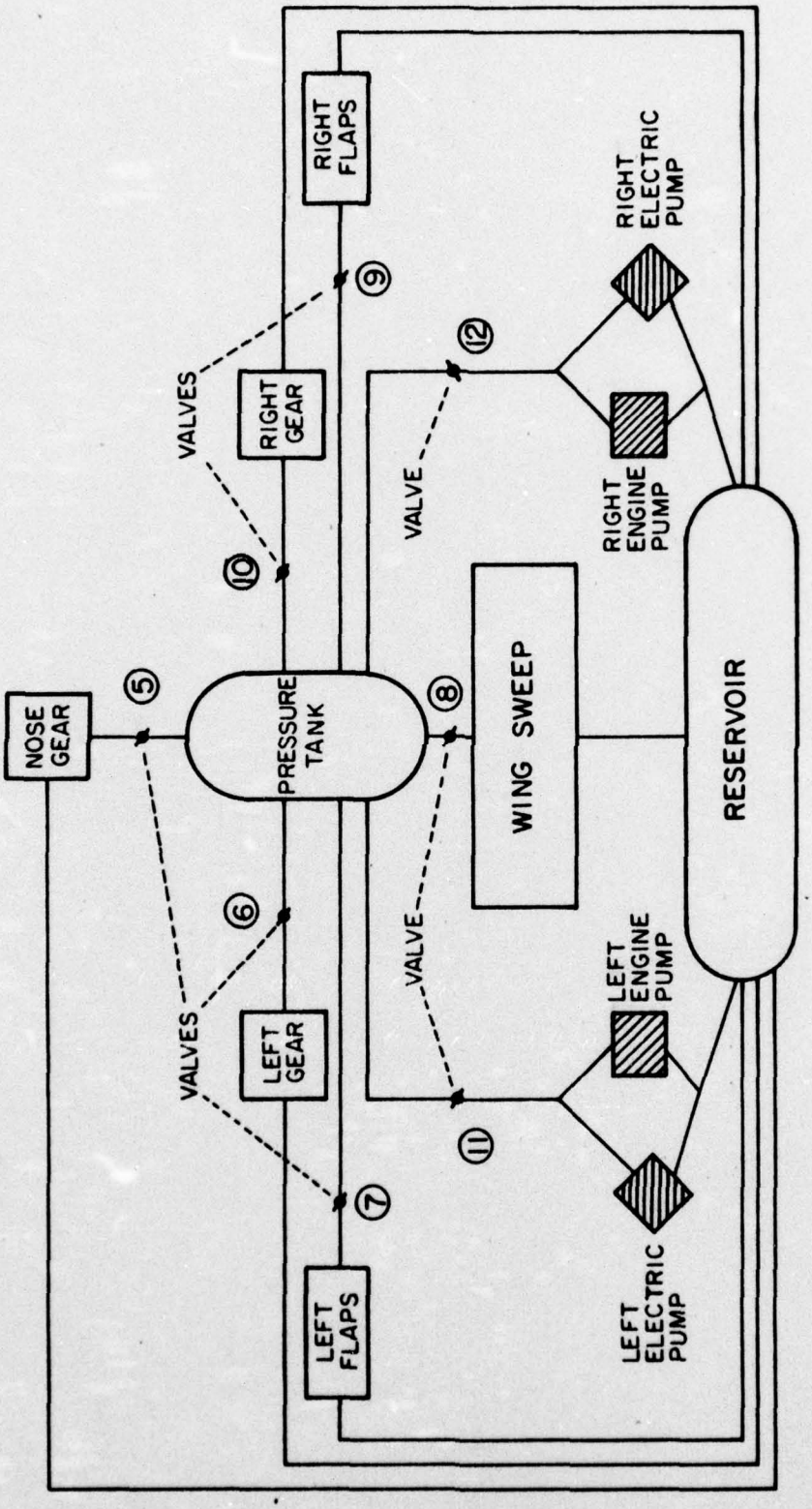

Figure 13. Simulated hydraulic system.

TABLE 10

Hydraulic System Simulation Activities

PHASE	FUNCTION	PARAMETER
INPUTS	STATES	DEMAND WING SWEEP ANGLE DEMAND FLAP ANGLE DEMAND LANDING GEAR STATE PUMPS VALVES
	COMMANDS	PILOT CADM
	CONSTRAINTS	GREMLIN OTHER SYSTEMS AIRSPEED
CALCULATES	PRESSURE SYSTEM	ACCUMULATOR TANK PRESSURE INDIVIDUAL LINE PRESSURES FLUID RESERVOIR LEVEL
	INFLUENCE	GREMLIN LEAKS
ACTIVATES	HYDRAULIC SYSTEM	WING SWEEP FLAPS LANDING GEAR
	INFLUENCE	GREMLIN OTHER SYSTEMS
OUTPUTS	STATES	PRESENT WING SWEEP ANGLE PRESENT FLAP ANGLE PRESENT LANDING GEAR STATE ACCUMULATOR TANK PRESSURE FLUID RESERVOIR LEVEL INDIVIDUAL LINE PRESSURES

Total system failure can come from the loss of the pumps, loss of pressure, jamming of valves, or the loss of hydraulic fluid because of leaks. Neither the landing gear nor the flaps can operate asymmetrically, although the electric motors can be used to activate one or more elements while the Hydraulic System activates the other(s). Valves and pumps operate in a network much like that of the Fuel/Engine System. Sensor data from the components of this system are provided for the pilot and the CADM through the Electrical System. Commands from the pilot and CADM to this system are also carried by the Electrical System.

The major component of the Hydraulic System is the accumulator pressure tank. Two engine and two electrically driven pumps pressurize this tank. The electric pumps work only when the engine driven pumps are off. If both pumps on one side are off, the pump on the other side can not pressurize the tank to maximum pressure. Without maximum pressure in the accumulator tank, the wing sweep mechanism will not function. One pump can, however, supply enough pressure to operate the flaps and landing gear.

In order to activate one of the subsystems, the valve in the hydraulic line leading to that subsystem device is opened. The pressure in that line is checked to indicate the presence of leaks in the line. If the line is pressurized, the component is activated. If a no-pressure condition is indicated, the controlling valve is closed and a signal is sent for the back-up electric motor controlling the device to be activated. If both the hydraulic and electric actuators for the particular device are out, the subsystem failure flag is set "on". This prevents asymmetric activation of the components of a subsystem.

For example, in the flap subsystem, when a flap activation signal is received, the pressure in the accumulator tank is checked. Then, if there is pressure in the tank, the valve to the left flap is opened. If the line is pressurized, the flap is set for activation. Then the right flap valve is opened and the pressure checked. If the line is at pressure, the flaps open to the desired angle. If either or both lines are unpressurized, the electric motors for the devices on the no-pressure lines are turned on, and the flaps open to the desired angle. Non-activation of both the actuators on one side causes the flap subsystem to fail. The flap subsystem failure flag is then set "on".

Six hydraulic lines return fluid from the actuators to the reservoir tank. If more than three of the lines have leaks or zero pressure, an insufficient amount of fluid is returned to the reservoir tank to feed the pumps pressurizing the accumulator tank. Insufficient fluid in the reservoir tank results in total Hydraulic System failure, as does a no-pressure condition in the accumulator pressure tank.

Total failure of the Hydraulic System does not have the immediately serious consequences of the total failure of the other two systems in AIRSYS. However, total failure of the Hydraulic System can have long range effects on mission success. A wing sweep angle of 70 degrees without flaps and perhaps without landing gear may not be serious in a cruise condition, but later in the mission when a landing is necessary, this aircraft configuration can have a very serious effect on safe mission completion.

CADM and the pilot have access to outputs from the Hydraulic System and the means to correct any non-hard jammed failures. Outputs from the Hydraulic System are as follows:

1. Accumulator tank pressure
2. Status of flaps, landing gear, and wing sweep
3. Status of pumps and valves
4. Hydraulic line pressures
5. Fluid reservoir level
6. Overall Hydraulic System status.

3.4 INTERACTION BETWEEN SYSTEMS

All three AIRSYS systems are heavily interconnected. Figure 14 shows how a typical command is transmitted from the pilot to an individual component and the response of the subsystems to the command. Failures in one system could result in failures in another, increasing the complexity of any solution to a problem. Also, because of these interactions, recognizing the source of a series of failures becomes more difficult. For example, as shown in Figure 15, the loss of an engine results in the loss of the engine driven fuel and hydraulic pumps as well as the electric generator attached to that engine. The loss of the generator can cause the loss of many components in all three systems. A list of these components lost due to the above failure is given in Table 11. Thus, the loss of an individual component of one system can cause the loss of components in another system and perhaps the entire system. The use of such an arrangement taxes the abilities of the pilot and the CADM to function separately and cooperatively.

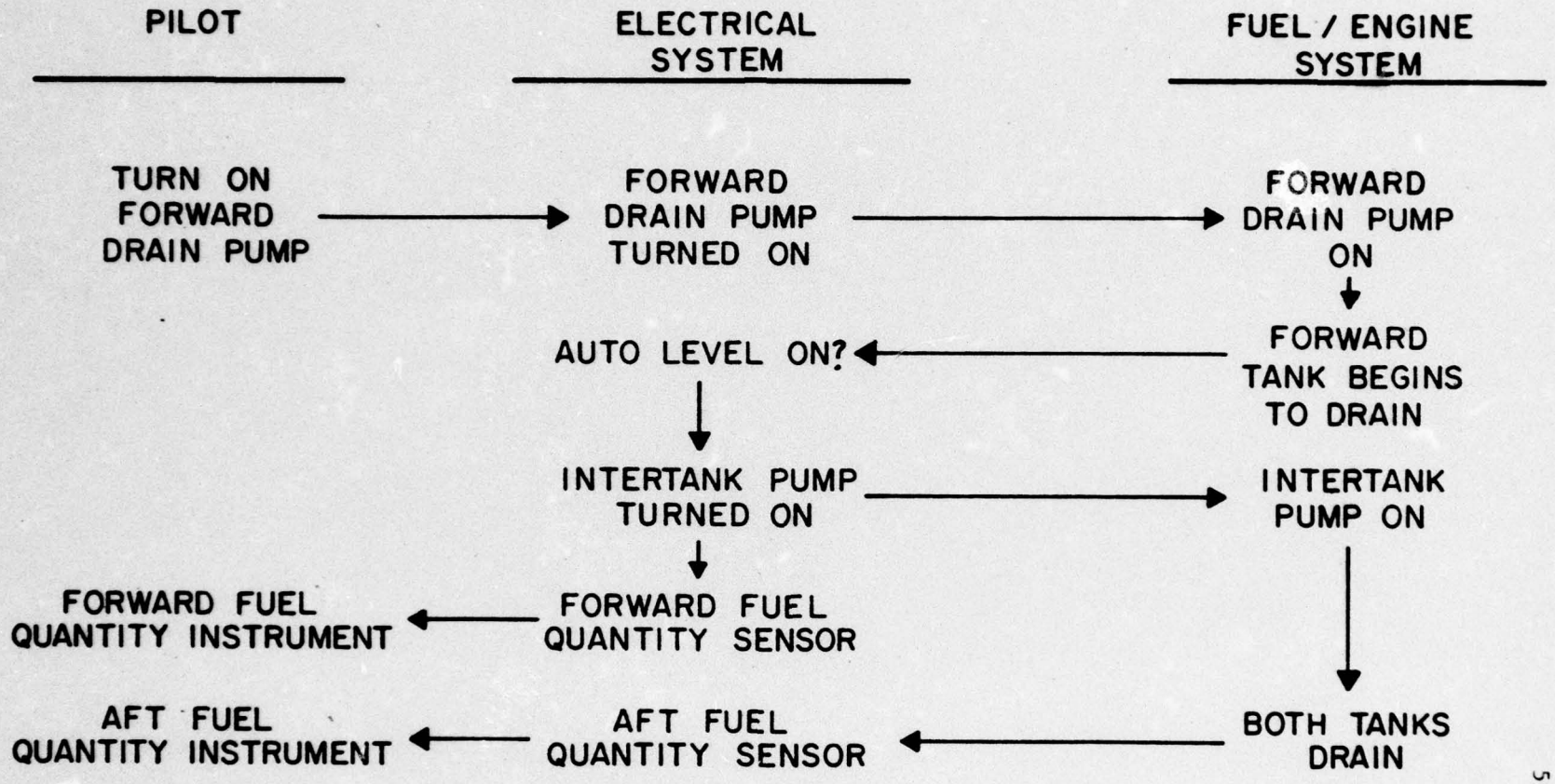

Figure 14. Typical AIRSYS activity.

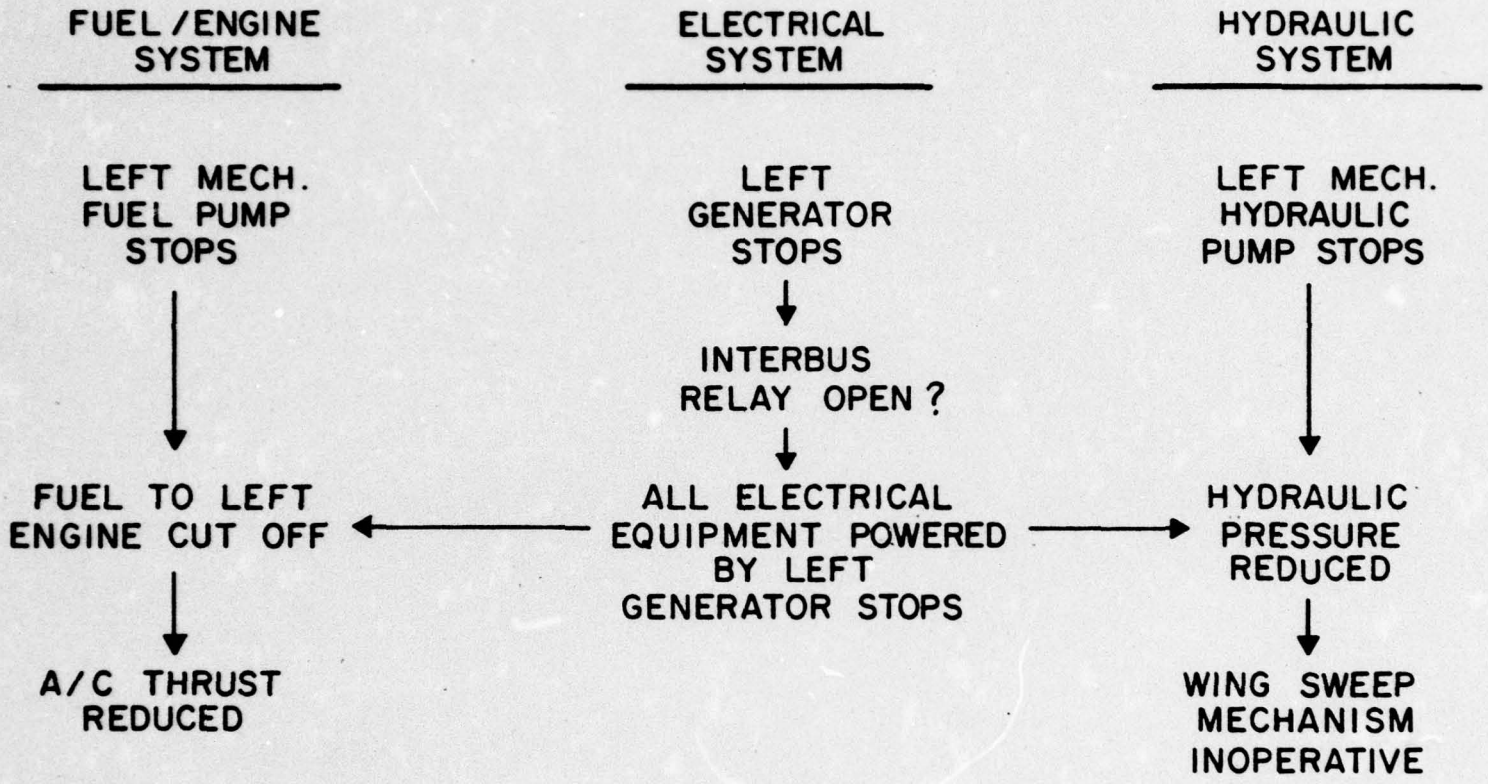

Figure 15. Consequences of component failure.

TABLE 11

Components Lost Due to Left Engine Destruction

FUEL/ENGINE SYSTEM	ELECTRICAL SYSTEM	HYDRAULIC SYSTEM
• FUEL VALVES (2)	• LEFT GENERATOR	• HYDRAULIC VALVES
• INTERTANK PUMP		• LEFT MECHANICAL HYDRAULIC PUMP
• REAR DRAIN PUMP		• LEFT ELECTRICAL HYDRAULIC PUMP
• LEFT MECHANICAL FUEL PUMP		• WING SWEEP MECHANISM
• LEFT ELECTRICAL FUEL PUMP		• FLAPS *
		• LANDING GEAR *

* POSSIBLE LOSS - DEPENDING ON VALVE STATES AT TIME OF FAILURE

The interaction between systems applies not only to system failures but also to component back-ups. The electric motors, in the flaps and landing gear, back-up hydraulic actuators for those subsystems, and the electric fuel and hydraulic pumps back-up the engine driven mechanical pumps. Cooperation between the systems and duplication of components offers the CADM and the pilot alternatives to total component and system failure.

4. CONTROLS AND DISPLAYS

The physical hardware of the simulator includes a joystick, two throttles, a touchtone keyboard to input and request data, a monitor display to display current subsystem states, and a vertical situation display (VSD). Figure 16 indicates the present physical hardware of the simulator.

The monitor display is based on the Hughes Master Monitor Display (MMD).[12] The MMD presents current AIRSYS information, as well as thrust levels and other sensor outputs to the pilot. It can also warn him of a failure or impending failure in the simulation. The MMD is the CADM's principal means of communication with the pilot. Figure 17 shows the MMD display and keyboard arrangement. Table 12 lists the method of calling information from the SDB.

The VSD displays aircraft pitch and bank angles through an artificial horizon. Heading is displayed on a compass. Altitude, airspeed, rate of climb, and command information are displayed on the VSD by means of bar

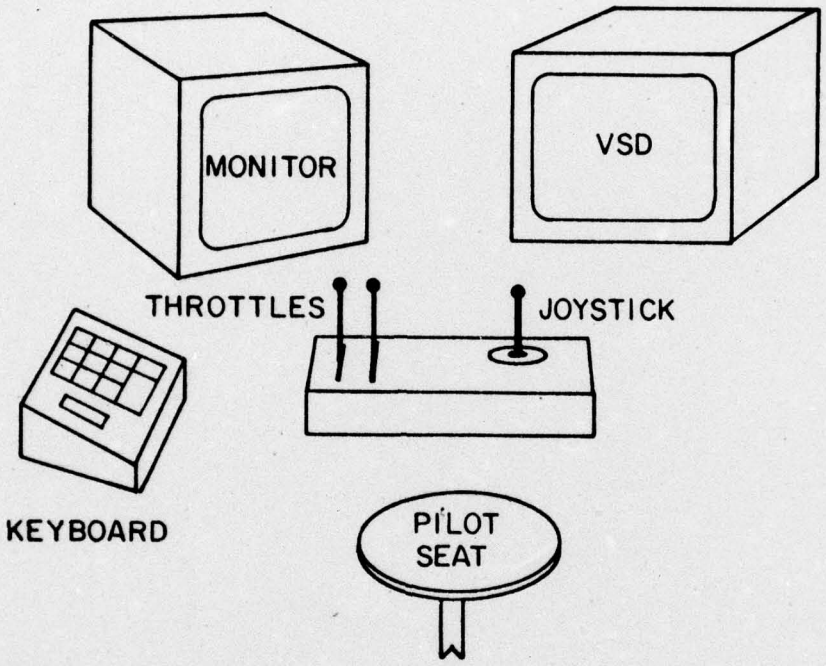

Figure 16. Simulator physical hardware.

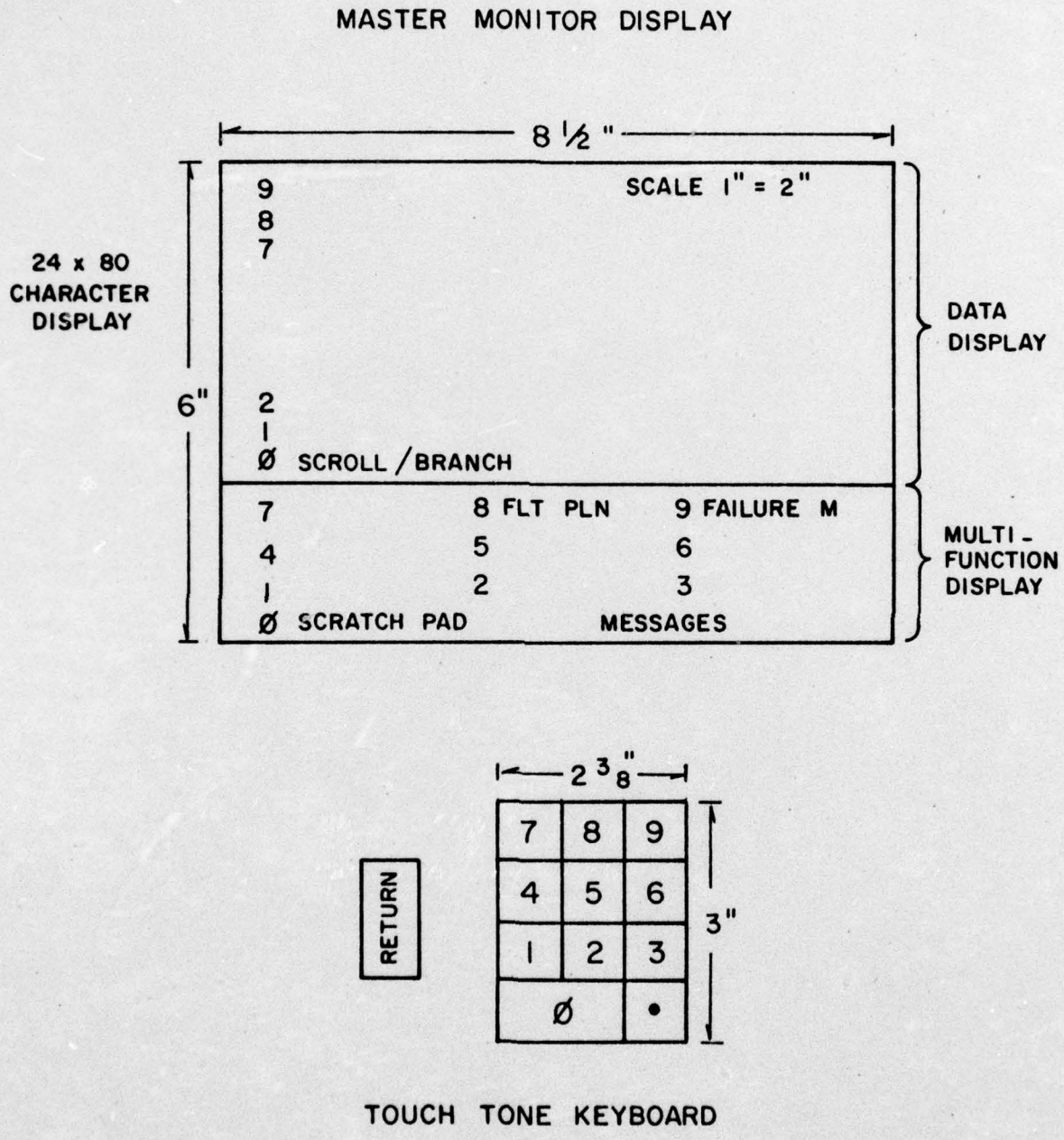

Figure 17. MMD and touchtone keyboard arrangement.

TABLE 12

Keyboard Entry Coding Method

SYMBOL	DEFINITION	USE
Ⓝ	CHARACTER	CHOICE OF MENU
Ⓡ	RETURN	TERMINATOR
⊙	DECIMAL	DELIMITER

EXAMPLES :

Ⓝ Ⓡ SPECIFIES A DATA DISPLAY OPERATION

⊙ Ⓝ Ⓡ SPECIFIES A MULTI-FUNCTION DISPLAY OPERATION

DATA CHANGES, FUNCTIONS IN USE, AND MESSAGES ARE INTENSIFIED FOR A PERIOD OF TIME.

graphs, alphanumeric symbols, and a moving aircraft symbol. Figure 18 shows the make-up of the VSD.

The joystick and throttles send signals to the SDB through an A/D signal converter. The aerodynamic model program reads the SDB and acts on these signals. The results of the reactions to these inputs are returned to the SDB where the VSD and the MMD read and display them to the pilot. The CADM also has access to this data in the SDB.

The touchtone keyboard is used by the pilot to input data and requests for data into the SDB. There, the other programs can read and act upon these pilot inputs. The pilot sees the result of his inputs on the MMD and the VSD. Through the keyboard, the pilot can change the wing sweep angle, the flap angle, and the gear state. He can also investigate or change the current state of any AIRSYS component and can correct a failure through the use of the appropriate code input to the keyboard.

5. RESULTS AND CONCLUSIONS

Tests on the aerodynamic model of the CADM simulator are described in Section 3.3 of this work. The results of these tests show that the model is responding correctly and is stable in all aircraft configurations and flight conditions. Analysis of the longitudinal and lateral mode experimental data shows good correlation with the predicted results. The aerodynamic model was found to be a suitable and adequate simulation of a variable geometry fighter aircraft, for the purposes of the CADM study. Flight experience with the simulator indicates that the flying

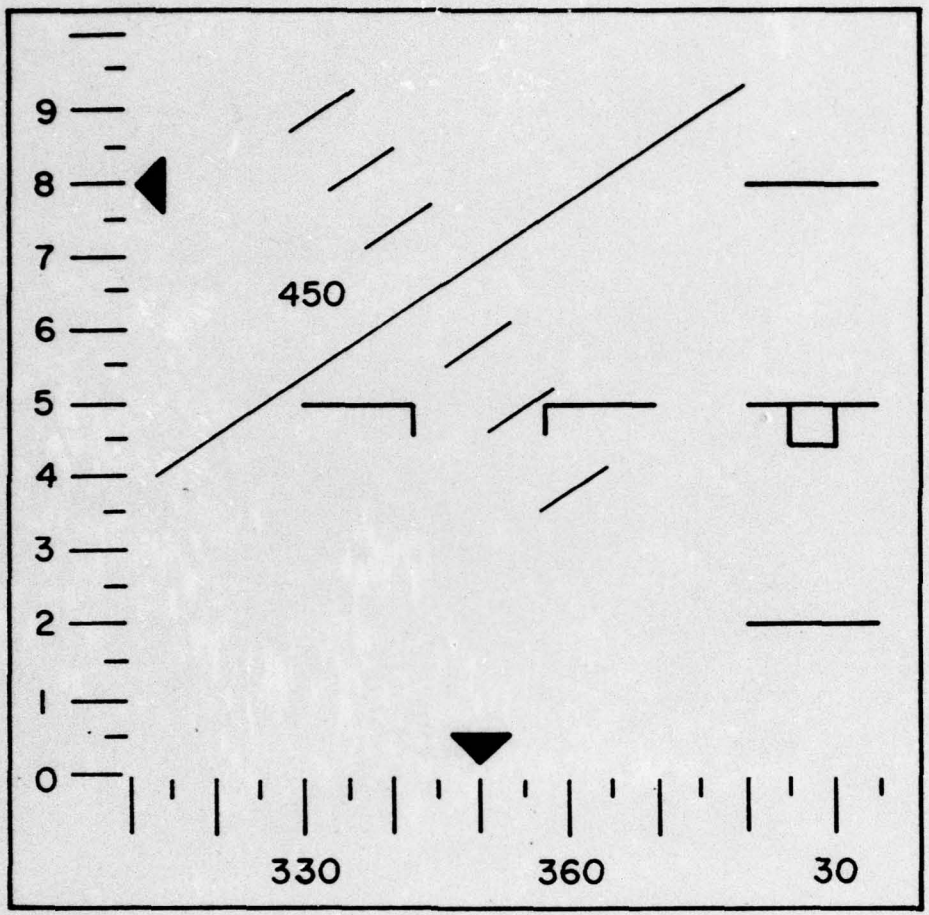

Figure 18. Vertical situation display.

task is fairly complex, with the ability to apply varying workloads on the pilot.

Testing of the AIRSYS is accomplished through the use of the MMD. While the nature of the AIRSYS does not allow for the collection of quantitative data, the functioning of the subsystems can be observed on the MMD screen.

By implementing failures into AIRSYS and observing the actions and reactions of the subsystem components, the functioning of AIRSYS and the individual components was confirmed. In all cases, AIRSYS performed as designed.

The work described in this thesis was performed in support of the CADM project. Its purpose was to provide an operating environment for the CADM. The design, testing, and operation of the CADM was not part of this thesis work. These aspects of the CADM project have been described elsewhere.[13] Tests on the entire system, CADM and environment, have been very encouraging. Even when faced with the complexity of failures possible in the simulator, the CADM has shown its ability to operate in an aircraft environment.

LIST OF REFERENCES

1. Aviation Research Laboratory. "Cockpit Workload Reduction Through Computer Assistance." Savoy, Ill.: Author, Institute of Aviation, University of Illinois, Proposal ARL-73-18, October, 1973.

2. Chien, R. T. "On the Importance of Program Intelligence to Advanced Automation in Flight Operations." Technical Report 1. Urbana, Ill.: Author, Coordinated Science Laboratory, University of Illinois, Contract F33615-73-C-1238, Computer-Aided Decision-Making for Flight Operations, December, 1973.

3. Premselaar, S. J., Hatcher, J. G., Richardson, R. L., Kinnamen, R. L., and Smith, W. D. "Integrated Information Presentation and Control System Study." Technical Report AFFDL-TR-70-79, Seattle, Wash.: Author, The Boeing Company, Military Airplane Systems Division, June, 1971.

4. List, B. H. "Study of the Information Management Aspects of Integrated Avionics." Report U1-130072-1, Dallas, Texas.: Author, Texas Instruments Inc., Equipment Group, January, 1969.

5. Irons, R. P., Jr., Lindquist, O. H., Schultz, R. L., et al. "Integrated Engine Instrumentation System Study-Energy Management Subsystem Investigation." Vol. II: System Basis Appendixes (A, B, D, E). Minneapolis, Minn.: Author, Honeywell, Inc., Systems and Research Division, Report 12591-FR1, April, 1970.

6. Etkin, B. Dynamics of Atmospheric Flight. New York: Wiley, 1972.

7. General Dynamics. "Computer Program Development Specification for Software for Avionic System Simulation and Dynamic Validation." Fort Worth, Texas: Author, General Dynamics Corporation, Convair Aerospace Division, Report FZM-6197, Revision A, March, 1974.

8. Digital Equipment Corporation. DEC System 10, FORTRAN-10 Language Manual, Second Edition (DEC-10-LFORA-B-D). Maynard, Mass.: Author, Digital Equipment Corporation, January, 1974.

9. USAF Aerospace Research Pilot School. "Stability and Control." Revised. Edwards Air Force Base, Calif.: Author, The United States Air Force, FTC-TIH-68-1002, September, 1968.

10. Stoddart, S. A. "A Flight Dyanmics Evaluation of a Singer-Link GAT-2 as a Quasi-Simulator with Control Modifications." Savoy, Ill.: Author, Aviation Research Laboratory, Institute of Aviation, University of Illinois, Technical Report ARL-71-13/AFOSR-71-4, June, 1971.

11. Lowe, W. W. "A Comparative Study of the Parameters Influencing the Flying Qualities of Light General-Aviation Aircraft." Unpublished Master's Degree Thesis, Urbana, Ill.: University of Illinois, 1972.

12. Hughes Aircraft Company. "Master Monitor Display Study." Final Report, Contract N62269-73-C-0138, Culver City, Calif.: Hughes Aircraft Company, Aerospace Group, Data Systems and Human Factors Department, January, 1974.

13. Chien, R. T. "Computer-Aided Decision-Making in Flight Operations." Technical Report 2, Urbana, Ill.: Author, Coordinated Science Laboratory, University of Illinois, September, 1975.

APPENDIX 1

AIRCRAFT CHARACTERISTICS

APPENDIX 1

AIRCRAFT CHARACTERISTICS

$\bar{c}$	9.16	ft
T/eng	15,000	lbs
wt, gross	55,000	lbs
wt, empty	35,000	lbs
Alt, max	80,000	ft
Mach no, max	2.2	-
S	550	ft^2
e_o	0.9	-
w/s, max	100	lb/ft^2

δ_f	10	20	30	40		deg
Λ	15	25	35	50	70	deg
AR	6.55	5.90	5.46	4.37	3.28	-
I_x	70000	70000	70000	45000	45000	slug ft^2
I_y min	260000	260000	260000	275000	275000	slug ft^2
I_y max	320000	320000	320000	335000	335000	slug ft^2
δ_e trim @450 fps	.0745	.061	.045	.00125	-.069	rad
$c.g._{ref}$	25	35	37	40	50	% chord
α_{trim}	.06	.066	.0726	.0985	.1306	rad
b	60	54	50	40	30	ft

APPENDIX 1 (continued)

Λ, deg	$C_{L_{max}}$ *	V_{stall}, fps
15	2.0	205
25	1.8	216
35	1.6	229
50	1.3	254
70	1.0	290

*without flaps. Add .2 to C_L for each 10^o flap

Λ, deg	T_{ss}, lb @450 fps
15	9565
25	8239
35	8240
50	6914
70	5589

APPENDIX 2

NON-DIMENSIONAL STABILITY DERIVATIVES AND COEFFICIENTS

APPENDIX 2

NON-DIMENSIONAL STABILITY DERIVATIVES AND COEFFICIENTS

Derivative	15	25	35	50	70
C_{m_o}	0.1701	0.1504	0.1401	0.11995	0.10004
$C_{L_{max}}$	2.0	1.8	1.6	1.3	1.0
C_{m_α}	-0.6	-0.8	-1.0	-1.2	-1.4
$C_{m_{\delta_e}}$	-1.8	-1.6	-1.5	-1.4	-1.2
C_{m_q}	-20.0	-25.0	-27.5	-20.0	-12.5
C_{L_α}	5.7	5.4	5.1	4.2	3.6
C_{L_q}	6.0	7.0	8.0	8.25	5.0
$C_{L_{\delta_e}}$	1.0	1.0	1.0	0.9	0.8
$C_{L_{\dot{\alpha}}}$	3.0	3.0	3.3	3.0	2.8
C_{L_o}	-0.0015	-0.0024	-0.00026	-0.000175	-0.00004
$C_{m_{\dot{\alpha}}}$	-4.0	-4.0	-5.0	-5.5	-6.5
C_{D_o}	0.06	0.05	0.05	0.04	0.03
$C_{D_{\delta_e}}$	0.029	0.029	0.029	0.027	0.028

APPENDIX 2 (continued)

$C_{l_{\delta_a}}$	-0.085	-0.085	-0.085	-0.0775	-0.0575
C_{l_p}	-0.4	-0.4	-0.5	-0.3	-0.2
$C_{L_{\delta_f}}$	1.1428	1.1428	1.1428	0	0
$C_{D_{\delta_f}}$	0.012	0.011	0.010	0	0
$C_{D_{\delta_g}}$	0.011	0.011	0.011	0.011	0.011
$C_{m_{\delta_f}}$	-0.024	-0.021	-0.02	0	0
$C_{m_{\delta_g}}$	-0.05	-0.05	-0.05	-0.05	-0.05

APPENDIX 3

SIMULATED FLIGHT TEST CONDITIONS

APPENDIX 3

SIMULATED FLIGHT TEST CONDITIONS

LONGITUDINAL MOTION

CONDITIONS	VARIABLES	NOTES
1-5	Λ	Λ = 15, 25, 35, 50, 70 deg
6-9	δ_f	$\Lambda = 15^o$ δ_f = 10, 20, 30, 40 deg
10-13	δ_f	$\Lambda = 25^o$ δ_f = 10, 20, 30, 40 deg
14-17	δ_f	$\Lambda = 35^o$ δ_f = 10, 20, 30, 40 deg
15-19	δ_f	Λ = 15, 25, 35, 50, 70 deg
		δg = 1 (extended)
20-22	c.g.	$\Lambda = 15^o$ cg = .20, .25, .30 chord
23-25	c.g.	$\Lambda = 25^o$ cg = .30, .35, .40 chord
26-28	c.g.	$\Lambda = 35^o$ cg = .32, .37, .42 chord
29-31	c.g.	$\Lambda = 50^o$ cg = .35, .40, .45 chord
32-34	c.g.	$\Lambda = 70^o$ cg = .45, .50, .55 chord
35-39	wt, Λ	Λ = 15, 25, 35, 50, 70 deg
		wt = 35000 lb

LATERAL MOTION

CONDITION	VARIABLE	NOTES
1-5	Λ	$\delta_a = 10^o$ Λ = 15, 25, 35, 50, 70 deg
6-8	δ_a	Λ = 25, $\delta_a = 1^o, 5^o, 10^o$